

pubs.acs.org/JPCC Article

# Operando Spectroelectrochemical Characterization Shows that the Dynamic Flow of Electrons through Melanin Involves Its Redox-State Switching

Eunkyoung Kim, Chen-yu Chen, Jun Wei Phua, Alessandra Napolitano, William E. Bentley, and Gregory F. Payne\*



Cite This: J. Phys. Chem. C 2023, 127, 19979-19994



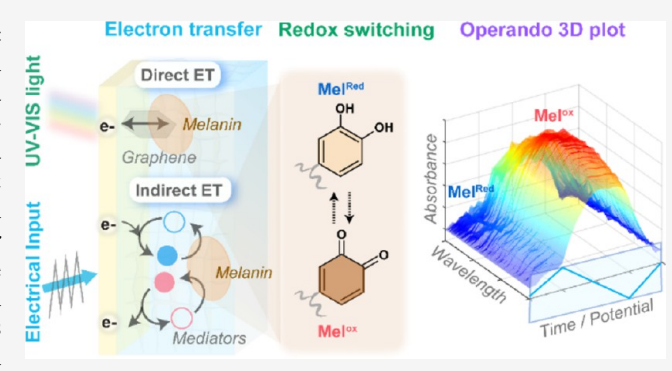
**ACCESS** I

III Metrics & More

Article Recommendations

Supporting Information

ABSTRACT: Melanin is a group of heterogeneous polymeric pigments that has been proposed to perform various biological functions and is attracting increasing technological interest as a sustainable electronic material for energy storage and bioelectronics. Here, we prepared a semitransparent hydrogel film from a soluble melanin obtained from the black soldier fly (Hermetia illucens; BSF) and applied an operando spectroelectrochemical approach to investigate the molecular-level changes that occur when electrons are "flowing" through this melanin (i.e., while electron transfer processes are "in operation"). Like other natural and synthetic melanins, we observed that the BSF melanin has reversible redox activities in the mid-physiological redox potential range. We report that electron transfer can occur through an



indirect (mediator-based) mechanism and also through a direct mechanism involving an extrinsic electron exchange with conducting graphene. In both mechanisms, we show that electron transfer is correlated to a reversible switching of the melanin's redox state. Finally, we provide evidence to support a chemical disorder model, which suggests that the properties of melanin may involve diverse structural and mechanistic features that occur over various length scales. Overall, we show that operando spectroelectrochemical measurements can bridge traditional bottom-up and top-down methods to facilitate the characterization of melanin.

# 1. INTRODUCTION

In biology, electron transfer reactions are integral to energy harvesting, biosynthesis, immune defense, and signaling, and there has been increasing technological efforts to promote electron exchange with biological systems for applications that include biofuel cells, bioelectrosynthesis, biosensing, and bioelectronics.<sup>8-17</sup> Scheme 1a illustrates that one area of particular recent interest involves the mechanisms for the export of electrons from microorganisms. It is well-established that electron export from cells can occur by an indirect mechanism of electron transfer (ET) in which electrons (i.e., reducing equivalents) are transported by diffusible metabolic products (e.g., hydrogen and formate in methanogenesis or sulfur in anaerobic methane oxidation)<sup>18,19</sup> or redox-active electron shuttles (e.g., flavins, humic substance, phenazine, and anthraquinone disulfonate). 10,20,21 Recent studies are also revealing a direct ET mechanism, 20,22-25 which involves the production of specialized cell-produced proteins (e.g., extracellular cytochromes and cell appendages pili). 18,19,25,26

While describing ET as direct or indirect is helpful, it cannot always capture the complexity associated with electron "flow" through biomolecular systems. One example is the natural pigment, melanin, which confers diverse biological functions

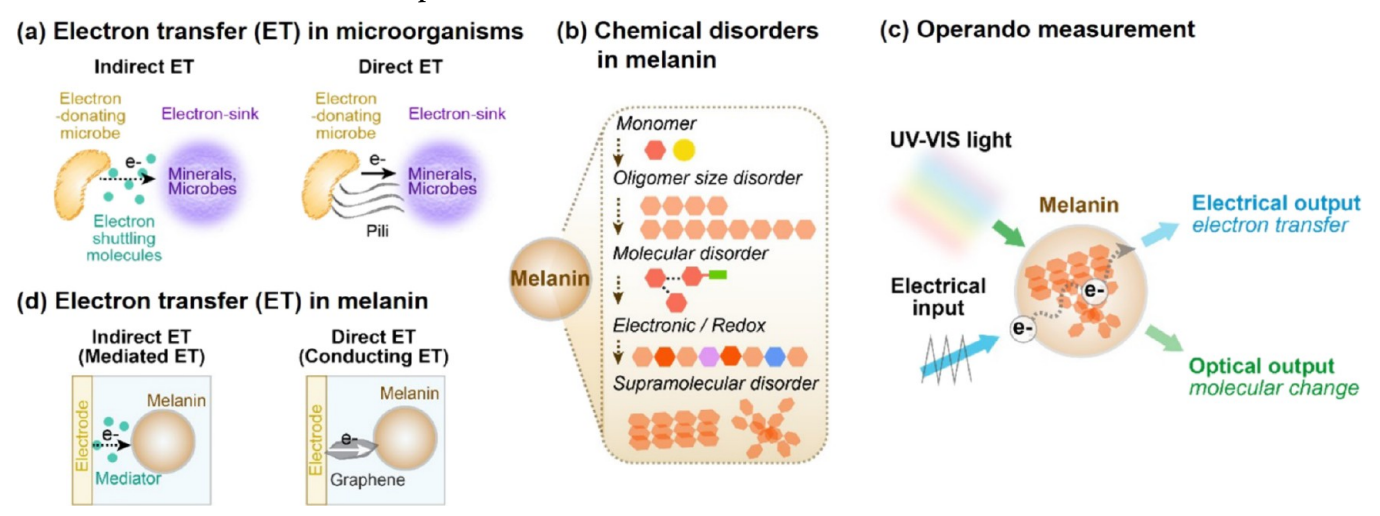
that result from its electronic properties (e.g., photo and antioxidant protection and metal binding). <sup>27,28</sup> In fact, melanin's electronic properties have attracted attention for decades as a potential sustainable natural candidate for solar energy conversion, <sup>29,30</sup> electrochemical energy storage, <sup>29,31–37</sup> and bioelectronics. <sup>38,39</sup> While electron flow through melanin is not yet fully understood, two mechanisms have been proposed. McGinness et al. <sup>40</sup> first reported the reversible electrical switching properties of eumelanin and suggested this material to be a naturally occurring amorphous organic semiconductor. Another mechanism proposed by Meredith and co-workers is that eumelanin possesses a hydration-dependent mixed ionic—electronic conductivity. <sup>41–43</sup> These authors demonstrated that the adsorption of water causes the generation of extrinsic free radicals and hydronium ions following a comproportionation

Received: July 26, 2023 Revised: August 30, 2023 Published: September 28, 2023





Scheme 1. (a) ET Mechanisms Used by Microorganisms to Export Electrons; Indirect ET Is Mediated by Diffusible Shuttles and Direct ET Involves Specialized Cell Appendages (e.g., Pili). (b) Melanin's Chemical Disorder Can Occur over Varying Length Scales. (c) Overview of Operando Spectroelectrochemical Measurements. (d) Suggested ET Mechanism for Melanin: Mediator-Based Indirect ET and Graphene-Based Direct ET



reaction between hydroquinone and quinone, thereby inducing hybrid ionic—electronic behavior. 42,44–48 Interestingly, both mechanisms suggest that the ET in melanin is associated with the  $\pi$ -conjugated structure of melanin and dynamic changes between a reduced state and an oxidized state of melanin. Thus, the ability of melanin to switch redox states may be important not only for its conductivity in technology but also for its biological functions.

Traditionally, the characterization of complex biomolecular systems starts by resolving the molecular structure and then relates structural features to functional properties. This bottom-up approach has been less successful for understanding the complex electronic properties of melanin. In fact, a "chemical disorder model" was proposed that explains the melanin's broad and featureless absorption spectrum in terms of a heterogeneous mix of structural subunits. 52,53 Even bottom-up synthetic studies starting from well-defined precursors have yielded diverse chemically complex melanins, 54-57 leading to the suggestion illustrated in Scheme 1b that chemical disorder can include the monomer type; the oligomer size and structure; the electronic (i.e., redox) states; and the supramolecular organization. An alternative, top-down, experimental approach focuses on functional properties (e.g., metal binding, 32,58-60 optoelectronic 61,62 and energy storage<sup>32,63,64</sup>). In the short term, a focus on function (vs chemical structure) is more directly linked to applications. In the long term, complementary top-down and bottom-up approaches should facilitate the mapping of the molecular structure to functional properties.

Recently, a variety of experimental methods have been developed that partially bridge bottom-up chemical analysis and top-down functional analysis for electronic materials. Specifically, these "operando" methods aim to reveal structure—activity relationships by simultaneously observing molecular-level changes (e.g., using spectroscopic and imaging techniques) while ET processes are occurring (i.e., while the material is "in operation"). 65–68 In technology, operando approaches are being used to understand reaction mechanisms, reveal mechanisms of materials degradation, and guide the development of new materials for improved device perform-

ance. $^{66-68}$  Operando approaches are also being used in studies with biological systems $^{69,70}$  such as the elucidation of the enzymatic redox reaction mechanisms. $^{71}$ 

Here, we used an operando approach illustrated in Scheme 1c to simultaneously monitor the molecular-level changes that occur when electrons are "flowing" through melanin. For these studies, we used a soluble natural melanin extracted from the cuticle of the black soldier fly (Hermetia illucens; BSF). 54,72 This BSF melanin is synthesized during insect sclerotization (i.e., hardening), and thus, its biological source and function are different from melanosome-generated melanins. Further, this BSF melanin is obtained from invertebrate biomass followed by the demineralization using acid treatment and the deproteination using a strong base treatment, 72 which may alter its native structure. 73 Because of its solubility, it was possible to prepare a partially transparent hydrogel film with BSF melanin and to perform operando analysis by probing this film's electronic properties while simultaneously observing changes in redox-state-dependent spectral properties. Despite being a relatively simple naturally derived material, the BSF melanin retains the complex structural and functional properties that are characteristic of melanin. Using the terminology from microbiology, Scheme 1d shows that we used diffusible mediators to characterize indirect ET, and we used graphene to "wire" the BSF melanin to the electrode to investigate direct ET. We demonstrate that BSF melanin is reversibly redox active and that ET through either direct or indirect ET mechanisms is associated with a switching of the BSF melanin's redox state. We also provide evidence consistent with a heterogeneous population of redox-active melanin species.

## 2. METHODS

**2.1. Chemicals and Materials.** The following materials were purchased from Sigma-Aldrich (St. Louis, MO): chitosan (85% deacetylated), Ru(NH<sub>3</sub>)<sub>6</sub>Cl<sub>6</sub> (Ru<sup>3+</sup>), and catechol. Ferrocene dimethanol (Fc) was purchased from Alfa Chemistry (Ronkonkoma, NY). Graphene (N002-PDR) was purchased from Angstron Materials (Dayton, OH). Black soldier fly (*Hermetia illucens*; BSF) melanin powder was

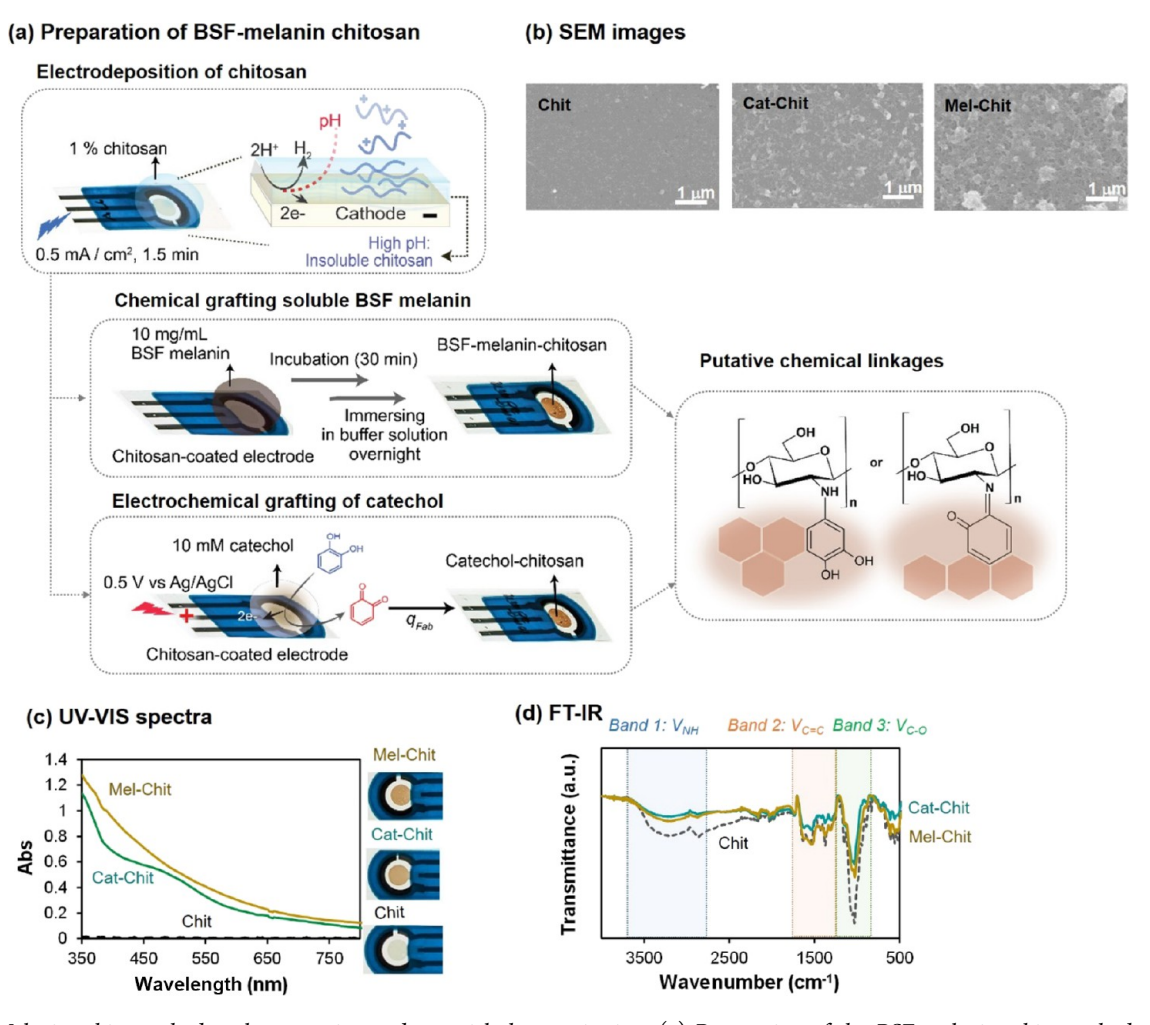


Figure 1. Melanin—chitosan hydrogel preparation and material characterization. (a) Preparation of the BSF melanin—chitosan hydrogel (Mel-Chit)-coated electrode showing (i) electrodeposition of chitosan hydrogel, (ii) chemical grafting of BSF melanin, and (iii) electrochemical grafting of catechol into the chitosan-coated electrode. (b) SEM images, (c) UV—vis spectra, and (d) FT-IR spectra for the film-coated electrodes.

supplied by Insectta (Pte. Ltd., Singapore). S4,72 BSF melanin solution was prepared by dissolving BSF melanin into 0.1 M phosphate buffer solution (pH 7.0) and then passing the melanin solution through a 0.2  $\mu$ m filter to remove insoluble particulates. Chitosan solution (1%, pH ~5.5) was prepared by dissolving chitosan flakes in deionized water, and the pH was adjusted using 2 M HCl. The solutions of the mediator were prepared in phosphate buffer (0.1 M; pH 7.0). Deionized water (>18 M $\Omega$ ) was obtained from the Super-Q water system (Millipore). A transparent gold electrode was purchased from Metrohm (Riverview, FL) and was used for a spectroelectrochemical experiment. A standard gold electrode was purchased from CH Instruments (Austin, TX) and was used for the electrochemical characterization.

**2.2.** Preparation of Various Film-Coated Electrodes. 2.2.1. Preparation of Chitosan or Graphene—Chitosan Film-Coated Electrodes. A thin-film-coated electrode was prepared by dropping 100  $\mu$ L of a chitosan solution (1 w/v%) or a mixed solution of chitosan (1%) and graphene (0.5 w/v%, low content) on a transparent gold electrode (r = 0.2 cm) and then applying the constant current density (0.5 mA·cm<sup>-2</sup>) for 1.5 min using a chronopotentiometry technique. A thin-film-coated electrode was used for the spectroelectrochemical, SEM, and FT-IR measurement.

A thick-film-coated electrode was prepared by immersing a standard gold electrode ( $r=0.1~\rm cm$ ) into either a chitosan solution (1%) or a mixed solution of chitosan (1%) and graphene (1%, high content) and imposing a constant current density of 0.5 mA·cm<sup>-2</sup> for a comparatively longer time (3 min) using a chronopotentiometry technique. A thick-film-coated electrode was used for the electrochemical characterization.

2.2.2. Chemical Grafting of Melanin or Electrochemical Grafting of Catechol. For the preparation of melaninchitosan (Mel-Chit) or melanin-graphene-chitosan (Mel-Gr-Chit) coated electrodes, the Chit or Gr-Chit film-coated electrode was placed into 2.5 or 10 mg/mL melanin dissolved in phosphate buffer solution (0.1 M, pH 7.0) and incubated for 30 min, as shown in Figure 1a. After that, the resulting electrode was washed with excess water and immersed into buffer solution overnight to remove the excess melanin physically bound to the electrode. For the electrochemical grafting of catechol, the Chit or Gr-Chit hydrogel-coated electrode was placed into 10 mM catechol solution (0.1 M phosphate buffer, pH 7.0) and then a constant potential (0.6 V vs Ag/AgCl) was applied to reach a  $q_{\text{Fab}}$  of 0.16 C·cm<sup>-2</sup>, as shown in Figure 1a. Then, the Cat-grafted hydrogel-coated electrode was washed with excess water to remove the physically bound catechol.

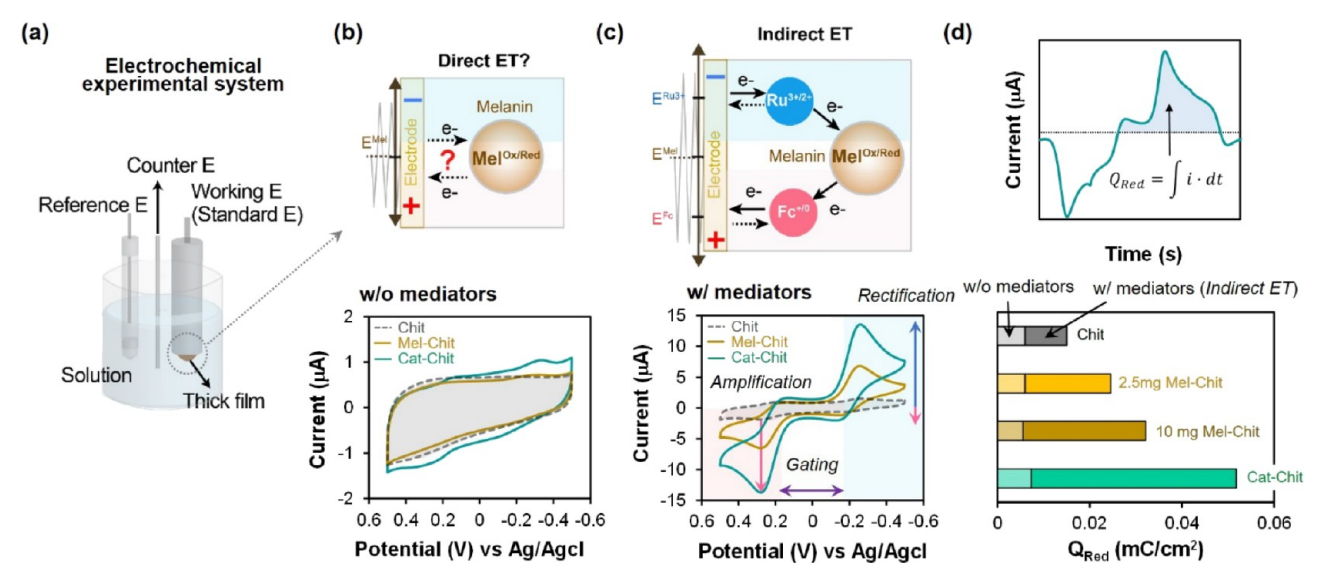


**Figure 2.** Electrochemical characterization of indirect ET in Mel-Chit. (a) Schematic of the electrochemical experimental system using a thicker-film-coated standard gold electrode. (b) Cyclic voltammograms (CVs) of Chit-, Mel-Chit-, and Cat-Chit-coated standard electrodes measured in 0.1 M phosphate buffer (pH 7.0) at a scan rate of 100 mV/s. (c) CVs of the three film-coated electrodes measured in the presence of mediators (0.1 mM Fc, 0.1 mM Ru<sup>3+</sup>, 100 mV/s). (d) Effect of melanin content on the reductive charge by the indirect ET pathway.

**2.3. Electrochemical Measurement.** A thick hydrogel film was electrodeposited on a standard gold electrode, and cyclic voltammetry measurements were made using a three-electrode system with Ag/AgCl as a reference electrode and Pt wire as a counter electrode. As described in Figure 2a, all three electrodes were placed into an electrochemical cell containing the phosphate buffer solution (0.1 M, pH 7.0) without or with mediators of 0.1 mM Fc and 0.1 mM Ru<sup>3+</sup>. Air was excluded by purging N<sub>2</sub> during the experiment.

2.4. Operando Measurement. Transparent gold electrodes coated with thin electrodeposited hydrogel films were placed into a cuvette that was filled with the phosphate buffer solution (0.1 M, pH 7.0) without or with mediators of 0.2 mM Fc and 0.2 mM Ru<sup>3+</sup>. A platinum wire was used as a counter electrode and Ag/AgCl was used as a reference electrode. All three electrodes were connected to an electrochemical analyzer. Air was excluded by purging N2 during the experiment (note: Figure S1 of the Supporting Information shows the picture of the spectroelectrochemical system). The optical absorbance was monitored over time with a UV-vis spectrophotometer (AvaSpec-ULS2048, Pine Research). The optical absorbance data was used after the data processing of an adjacent averaging. Simultaneously, the optical (absorbance) and electrochemical (current) output responses were individually recorded over time.

**2.5.** Instrumentation. 2.5.1. Electrochemical Analysis. For the electrodeposition of Chit or Gr-Chit hydrogels, a constant current density was applied by performing chronopotentiometry using a CHI6273C electrochemical analyzer (CH Instruments). A multichannel electrochemical analyzer (CHI1040C, CH Instruments) was used for the electrochemical characterization. An electrochemical analyzer (CHI620E, CH Instruments) was used for a spectroelectrochemical measurement (i.e., operando measurement).

2.5.2. Material Characterization. For the structural characterization, the samples were prepared by freeze-drying the hydrogel-coated transparent electrode. The images of hydrogel samples were obtained using a scanning electron microscope (SEM, SU-70, Hitachi, Pleasanton, CA). Chemical

characterization was performed using Fourier transform infrared spectroscopy (FT-IR, VERTEX 70 FT-IR, Bruker).

### 3. RESULTS

3.1. Material Characterization. Figure 1a shows the method used to coat an electrode with a chitosan-based hydrogel film containing BSF melanin (Mel-Chit). First, a thin chitosan hydrogel (Chit) is electrodeposited from a chitosan solution (1%; pH 5.5) onto a transparent gold electrode by applying a constant cathodic current (0.5 mA/cm<sup>2</sup>; 1.5 min). 742-76 Next, a phosphate-buffered solution (0.1 M; pH 7) containing soluble BSF melanin (either 2.5 mg or 10 mg/ mL; 100  $\mu$ L) was dropped onto the chitosan-coated electrode and incubated for 30 min in the air. After incubation, the Mel-Chit-coated electrode is washed extensively with water and placed into the buffered solution overnight to remove the physically entrapped melanin from the chitosan hydrogel. For comparison, we also prepared a control hydrogel containing catechol and chitosan (Cat-Chit) by first cathodically depositing chitosan and then anodically grafting catechol, as shown in Figure 1a. The putative linkages in Figure 1a suggest that Michael-type addition and Schiff base reactions are responsible for coupling catechol and melanin to the amine group of chitosan hydrogel."

To characterize the microstructure of these hydrogel electrode coatings, we used scanning electron microscopy (SEM). The SEM images in Figure 1b show that the Chitcoated electrode has a featureless flat microstructure, while the Cat-Chit- and Mel-Chit-coated electrodes show a rough morphology with 200–500 nm pores. The pore structure of Cat-Chit and Mel-Chit hydrogels may be due to the chemical grafting of catechols and melanins to the chitosan hydrogel.

For chemical characterization of these three hydrogels, we used UV-vis and FT-IR spectroscopies. Figure 1c shows the UV-vis spectra and photographs for the electrodes coated with the three hydrogels. The Chit-coated electrode was clear and showed very low absorbance, while both the Cat-Chit- and Mel-Chit-coated electrodes were brown-colored and showed a broad absorption over the whole range of wavelengths

consistent with melanin-like materials. 27,80 As expected for a true melanin, the spectrum for the Mel-Chit hydrogel film appears almost featureless, which likely arises from a high degree of heterogeneity of the structural moieties and possibly variable oxidation states of these moieties.<sup>81</sup> The absorption peak around 400 nm observed in the spectrum of the Cat-Chit film can be attributed to quinonoid species (e.g., aminoquinones or quinonimines), as illustrated in Figure 1a. 82,83 These results suggest that the grafted melanin and catechol may have similarly complex, but somewhat different, chemical structures. The FT-IR spectra in Figure 1d show that both the Cat-Chit and Mel-Chit hydrogels (compared to the Chit hydrogel) show some attenuation of band 1 (-OH and -NH stretching vibrations) and band 3 (C-O stretching vibrations) and no attenuation of band 2 (C=C stretching vibration of benzene), which provides support for some catecholic-based modification of chitosan. <sup>28,84</sup>

**3.2. Electrochemical Characterization for ET Mechanisms.** *3.2.1. Indirect ET in Mel-Chit.* We employed electrochemical methods to characterize the ET mechanisms for BSF melanin. For initial electrochemical characterization, a thicker Mel-Chit-coated electrode was prepared by depositing chitosan hydrogel onto a nontransparent, standard gold electrode for a longer time (3 min) using a constant current density of 0.5 mA/cm² and then reacting with melanin solution for 30 min. In addition, thicker Chit- and Cat-Chit-coated electrodes were prepared as negative and positive controls, respectively.

First, to check the possibility of a direct ET between melanin and the electrode (illustrated in the schematic of Figure 2b), a Mel-Chit-coated standard gold electrode was placed in a phosphate-buffered solution (0.1 M, pH 7.0) and cyclic voltammetry (CV) measurements were performed. The electrochemical experimental system is shown in a schematic of Figure 2a. The CV results in Figure 2b for the Mel-Chit-coated electrode and the Chit-coated electrode are very similar, while the CV results for the Cat-Chit-coated electrode show very small redox peaks (reduction at -0.3 V and oxidation at +0.25 V). These results indicate that the Mel-Chit film is nonconducting and that melanin species grafted within the thick hydrogel film do not directly exchange electrons with the electrode (note that the Cat-Chit control hydrogel also possesses minimal conducting properties).

Next, CV experiments were performed, while the hydrogel film-coated electrodes were immersed in a solution containing two mediators of 0.1 mM Ru(NH<sub>3</sub>)<sub>6</sub>Cl<sub>3</sub> (Ru<sup>3+</sup>) and 0.1 mM ferrocene dimethanol (Fc). A schematic of Figure 2c illustrates that these mediators can diffuse through the hydrogel films<sup>85</sup> and undergo thermodynamically controlled indirect ET mechanisms with melanin: Ru3+ mediates the transfer of electrons from the electrode to melanin, and Fc mediates the transfer of electrons from melanin to the electrode. The CV results in Figure 2c show that the Mel-Chit hydrogel shares three features with the Cat-Chit hydrogel (the positive control). First, current peaks are observed at the mediator's redox potentials: mediators act as voltage gates that allow electron flow to/from the melanin. Second, the Fc-oxidation and Ru<sup>3+</sup>-reduction peaks are amplified (compared to the negative Chit-film control): these amplifications result from the oxidative redox cycling of Fc and reductive redox cycling of Ru<sup>3+</sup>. Third, the mediator currents are rectified: Fc-oxidation (but not Fc<sup>+</sup>-reduction) is amplified, and Ru<sup>3+</sup>-reduction (but not Ru<sup>2+</sup>-oxidation) is amplified. This rectification, amplification, and gating of currents are characteristic features that indicate that although the Mel-Chit hydrogel is not conducting, the BSF melanin within the hydrogel is redox active and can undergo indirect ET with the diffusible mediators. We should note that the observed quantitative differences (i.e., differences in peak currents) in the CVs for Cat-Chit and Mel-Chit hydrogel films may reflect differences in the numbers of redox-active moieties present in the two films.

To further support the conclusion that BSF melanin is redox active, we prepared Mel-Chit-coated electrodes using two different concentrations (2.5 or 10 mg/mL melanin) and performed a CV experiment in the presence of both mediators. For quantification of redox activity, the reduction charge ( $Q_{\rm Red}$ ) was calculated by integrating the reduction current over time, as shown in Figure 2d. The bar graph in Figure 2d shows that the reduction charge of Mel-Chit in the presence of mediators increases as more melanin is grafted to the chitosan hydrogel.

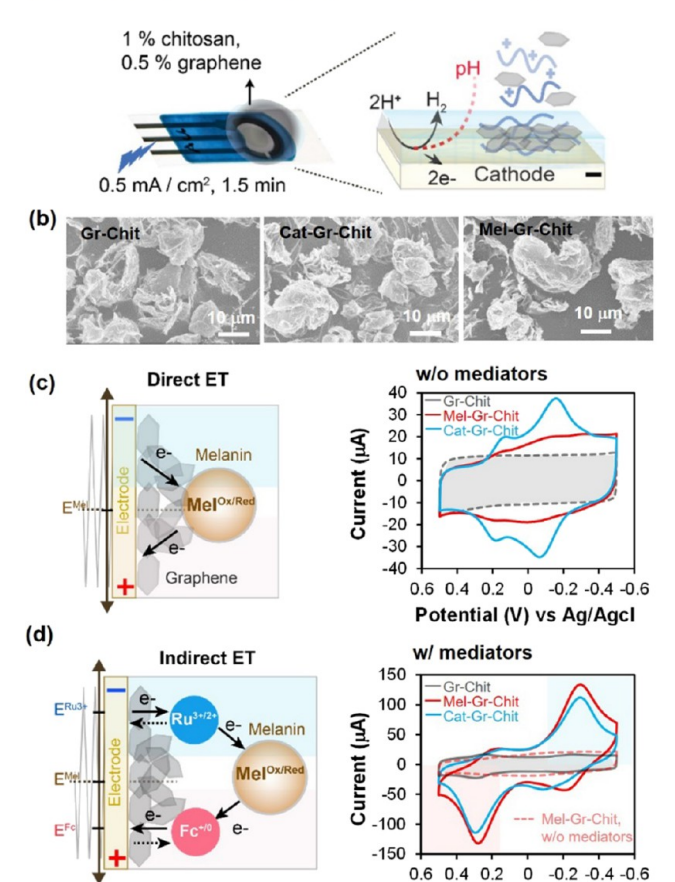
In summary, the results in Figure 2 indicate that the BSF melanin is redox active and can undergo indirect ET with these mediators, which is consistent with measurements from natural eumelanin from *Sepia*, DHN fungal melanin, and melanins from human hair.<sup>87–89</sup>

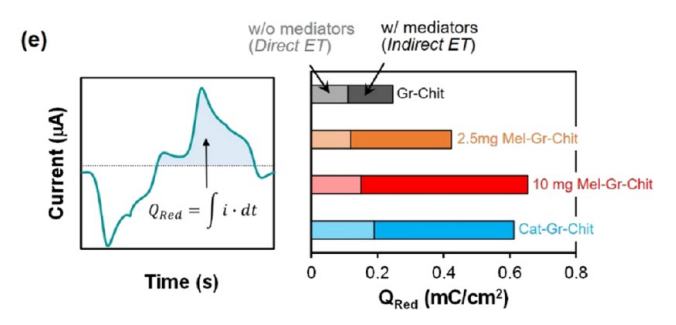
3.2.2. Direct ET and Indirect ET in Mel-Gr-Chit. Previously, we observed that when graphene was incorporated into a Cat-Chit hydrogel, it allowed direct ET between the electrode and the grafted catechol moieties (without the use of mediators). We next tested whether graphene could "wire" the hydrogel-grafted BSF melanin for direct ET. Figure 3a shows the method for electrodepositing a thinner graphene—chitosan hydrogel film (Gr-Chit) on the transparent electrode by dropping a chitosan solution (1%, w/v) mixed with graphene (0.5%, w/v) onto the electrode and applying a constant cathodic current (0.5 mA/cm²) for 1.5 min. After that, we used the same methods shown in Figure 1a to create film-coated electrodes with grafted BSF melanin (Mel-Gr-Chit) and grafted catechol (Cat-Gr-Chit).

Figure 3b compares the SEM images of the Gr-Chit-, Cat-Gr-Chit-, and Mel-Gr-Chit-coated electrodes. Compared to the SEM image in Figure 1b for the Chit hydrogel that lacked graphene, three SEM images of Figure 3b show the uniformly distributed and crumpled graphene flakes. However, there is no significant change in the SEM images of Mel-Gr-Chit and Cat-Gr-Chit compared to Gr-Chit hydrogels. The SEM image of Figure 3b indicates that the microstructure of graphene is maintained even after catechol or melanin grafting onto chitosan.<sup>90</sup>

We first investigated the role of graphene on the direct ET with BSF melanin, as shown in the schematic of Figure 3c. For this, a thicker Gr-Chit hydrogel film-coated electrode was prepared by placing a standard gold electrode into a chitosan solution (1%, w/v) mixed with higher graphene (1%, w/v) and applying a constant cathodic current (0.5 mA/cm²) for 3 min (longer time). The results from CV experiments using these electrodes are shown in Figure 3c, and the shapes of the CV curves suggest that both the Mel-Gr-Chit and Cat-Gr-Chit films confer ET activities that are not observed for the control Gr-Chit film, which shows a flat rectangular-shaped current response. This result is consistent with the conclusion that graphene enables direct ET between the grafted BSF melanin and the electrode. Another interesting finding is that the Cat-Gr-Chit shows two pairs of redox peaks, while the Mel-Gr-Chit

# (a) Electrodeposition of graphene-chitosan hydrogel





Potential (V) vs Ag/Agcl

Figure 3. Electrochemical characterization of direct and indirect ET in Mel-Gr-Chit. (a) Electrodeposition process of a thin graphene—chitosan hydrogel (Gr-Chit) on the transparent electrode. (b) SEM images for thin graphene—chitosan (Gr-Chit), catechol—graphene—chitosan (Cat-Gr-Chit), and melanin—graphene (Mel-Gr-Chit) film-coated electrodes. (c) CVs of three thick-film-coated standard electrodes measured in the phosphate buffer (100 mV/s) without mediators. (d) CVs of three thick-film-coated standard electrodes measured in the presence of mediators (0.1 mM Fc, 0.1 mM Ru<sup>3+</sup>, 100 mV/s). (e) Effect of melanin content on the reductive charge by both direct and indirect ET pathways.

shows a broad redox peak, which could be the result of multiple overlapping redox peaks. This broad "featureless" CV peak is consistent with a chemical disorder explanation that the BSF melanin may have multiple redox-active moieties that participate in ET. Thus, while we use the Cat-Chit and Cat-Gr-Chit films as positive controls to compare with the Mel-Chit and Mel-Gr-Chit films, the results indicate that there are qualitative differences in response characteristics that likely

reflect a more complex structure and chemistry for the melanin.

Next, we investigated ET when the Mel-Gr-Chit film was tested in the presence of mediators. Based on previous finding, 90 we hypothesize that the composite Mel-Gr-Chit film has two functional populations of BSF melanin: one population is wired to graphene to allow direct ET (as illustrated by the scheme in Figure 3c), and the second population is physically separated from graphene and can only participate in indirect ET with mediators (as illustrated by the scheme in Figure 3d). The CVs of Figure 3d show that both the Mel-Gr-Chit and the control Cat-Gr-Chit show the characteristic features of indirect and mediator-based ET (gating, amplification, and rectification). It is important to note the difference in the y-axis scales for the CVs in Figure 3c,d, and this difference indicates that while some of the BSF melanin can be wired by graphene for direct ET (red dotted line in Figure 3d), most of the grafted BSF melanin can only participate in indirect (mediated) ET.

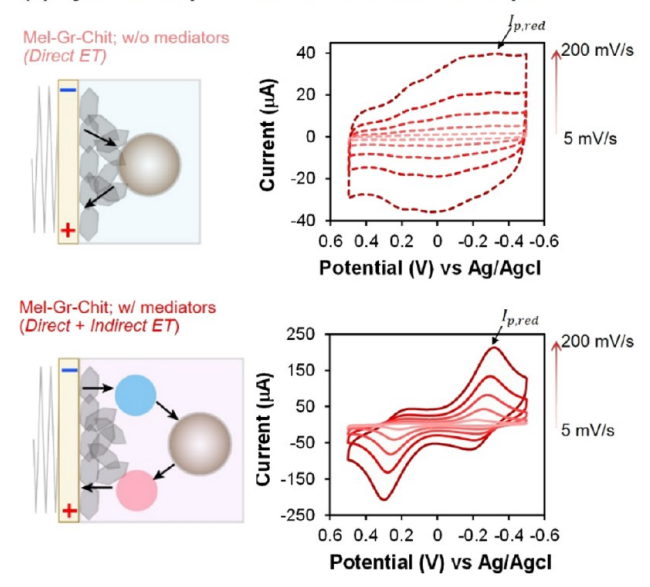
Using the same quantitative approach, as illustrated in Figure 2c, we compared the relative amount of direct and indirect ET for the Mel-Gr-Chit hydrogel. Figure 3e shows that as more BSF melanin is grafted into the Gr-Chit hydrogel, more electrons can be transferred through both direct and indirect ET mechanisms.

3.2.3. Dynamic Electrochemical Characterization. The above results indicate that BSF melanin that is grafted into a chitosan film can participate in indirect ET with diffusible mediators, while some of the BSF melanin can be wired by graphene to enable direct ET. To provide further support for these two ET mechanisms, we used a dynamic electrochemical technique in which CV measurements are made at different scan rates ( $\nu$ ). The first set of CV curves in Figure 4a examined direct ET and showed the responses when the Mel-Gr-Chit film was measured without mediators. The second set of CV curves examined indirect ET and showed the responses when the Mel-Gr-Chit was measured in the presence of mediators (0.1 mM Fc, 0.1 mM Ru<sup>3+</sup>). As expected, these CVs show that the redox peak current increases with scan rate [note: Figure S2 of the Supporting Information provides the additional CVs of Mel-Chit, Cat-Chit, Cat-Gr-Chit, and Mel-Gr-Chit in the absence and presence of mediators at different scan rates].

To quantify these dynamic responses, we plot the reduction peak current  $(I_{p,red})$  as a function of scan rate  $(\nu)$  using logarithmic scales. 92-95 As observed in Figure 4b, such plots are expected to be linear and this power-law dependence is often characterized by the slope and exponent (b). For electrochemical analysis, b approaches 1 for surface-controlled electrochemical processes (e.g., direct ET) and 0.5 for diffusion-controlled processes (e.g., indirect ET). 94,95,97 The table in Figure 4b shows that in the absence of mediators, the exponent for the Mel-Gr-Chit (b = 0.85) and Cat-Gr-Chit (b = 0.85) 0.88) suggests a direct ET mechanism. In the absence of graphene (direct ET is not possible) but presence of mediators, the exponent for the Mel-Chit (b = 0.49) and Cat-Chit (b = 0.46) suggests a diffusion-based indirect ET mechanism. Intermediate exponent values were observed when films were prepared with graphene and measured using mediators, which suggests that both direct and indirect ET mechanisms are occurring.

The conclusions from these electrochemical measurements are that BSF melanin is redox active, can participate in indirect

## (a) Dynamic responses of electrochemical outputs



### (b) Dynamic analysis of peak current changes

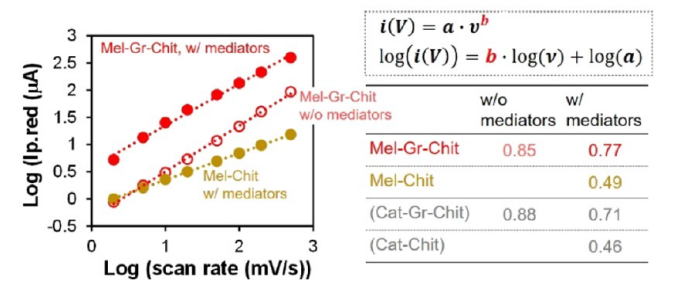


**Figure 4.** Dynamic electrochemical characterization. (a) CVs of the thicker Mel-Gr-Chit-coated standard electrode measured in the buffer solution without (upper plot) or with mediators (lower plot) by varying scan rate from 5 to 200 mV/s. (b) Dynamic analysis of peak current changes as a function of scan rate with table listing calculated by values

mediator-based ET, and can, in some cases, be wired by graphene to allow direct ET.

**3.3. Operando Measurement.** We next performed operando spectroelectrochemical measurements using the experimental system illustrated in Figure 5a that simultaneously observes spectral changes associated with redox-state switching while ET is occurring. We used a specially designed spectroelectrochemical system that allows  $N_2$  gas purging to our cuvette to remove the oxygen during the experiment. Our electrodes in this system are a thin-film-coated transparent gold working electrode, a Ag/AgCl reference electrode, and a platinum counter electrode.

For operando measurements, we typically impose an oscillating electrical input potential and monitor both the electrical output (i.e., current) associated with electron flow to/from the melanin and changes in optical spectrum associated redox-state switching of the BSF melanin. Figure Sb shows a three-dimensional plot obtained from these operando measurements and illustrates a constant  $\lambda$  slice and a constant E slice. As will be discussed, this three-dimensional plot shows the emergence of a broad absorption peak near 570 nm when the imposed potential is cycled into oxidative regions.

**3.3.1. Constant**  $\lambda$  **Slice: Redox Switching.** *3.3.1.1. Direct ET with Molecular Switching.* In the first operando study, we investigated direct ET and analyzed data from a constant  $\lambda$  slice. For this, we prepared a thin ( $\sim$ 5  $\mu$ m), partially transparent Gr-Chit hydrogel film on the transparent gold electrode, as illustrated in Figure 3a. After that, 100  $\mu$ L of melanin solution (2.5 mg/mL) was dropped on the Gr-Chit-coated electrode and was reacted for 30 min. For the spectroelectrochemical measurement, this thin-film-coated electrode was immersed in a cuvette containing phosphate buffer (PB; 0.1 M, pH 7.0), the cuvette was then placed into the instrument, and an oscillating potential input was applied to the electrode.

Figure 6a compares the time-series electrical and optical outputs for the Mel-Gr-Chit film to those for the negative control Gr-Chit film (shown in gray-dotted) [note: Figure S3 of the Supporting Information shows the time-series outputs for the positive control film, Cat-Gr-Chit]. The first output curve in Figure 6a is the electrical current. The Mel-Gr-Chit shows  $\sim$ 2-fold larger oscillating current amplitude ( $\Delta I_{ ext{Mel-Gr-Chit}}$ = 7.8  $\pm$  0.45  $\mu$ A) compared to the Gr-Chit ( $\Delta I_{\text{Gr-Chit}}$  = 3.6  $\pm$ 0.17  $\mu$ A). A second electrical output is the charge, which is calculated by integrating the current output over time  $(Q = \int$  $i \cdot dt$ ). The Mel-Gr-Chit shows that the output charge oscillates with a larger amplitude ( $\Delta Q_{\text{Mel-Gr-Chit}} = 0.81 \pm 0.013 \text{ mC}$ ) compared to that for the control Gr-Chit film ( $\Delta Q_{Gr-Chit} = 0.41$  $\pm$  0.042 mC). The higher electrical outputs of Mel-Gr-Chit (vs Gr-Chit) indicate that more electrons can be directly transferred to the Mel-Gr-Chit via graphene.

The third output in Figure 6a is the optical absorbance change at 570 nm. To generate a baseline for these optical measurements, we first poised each of these films (Gr-Chit or Mel-Gr-Chit) in their reduced state by imposing a reducing voltage (-0.5 V vs Ag/AgCl) for 2 min and measuring their UV-vis spectra. The UV-vis spectrum of the reduced state of Mel-Chit was used as the baseline. The absorbance in Figure 6a records the differential absorbance at 570 nm (A 570) relative to the baseline [note: the y-axis for absorbance is inverted to facilitate comparison with electrical output].99 While the control Gr-Chit shows no oscillations in the absorbance output ( $\Delta A_{Gr-Chit}$ ; ~0), the Mel-Gr-Chit shows a repeated oscillating absorbance output ( $\Delta A_{\text{Mel-Gr-Chit}}$ ; 0.0094  $\pm$ 0.0006). The dotted vertical lines in Figure 6a show that the maximum charge ( $Q_{\text{max}}$  reductive Q) occurs at the same time as the minimum absorbance ( $A_{\min}$ , a putative reduced catechol state), and the minimum charge  $(Q_{min}, oxidative Q)$  occurs at the same time as the maximum absorbance ( $A_{\text{max}}$ ), the putative oxidized quinone state). The correlation of these oscillating output responses provides direct evidence that ET through graphene is coupled to the redox-state switching of BSF melanin, as illustrated in the schematic of Figure 6b [note: this schematic suggests a catechol—quinone redox couple].

To further illustrate the correlation between electrical and optical outputs, we replotted the time-series data in Figure 6a as phase-plane plots, which display output responses vs input potential [note: the *y*-axis for absorbance is again inverted to facilitate visual comparison]. Figure 6c shows the phase-plane plots for electrical charge and optical absorbance. The blue-shaded region of Figure 6c illustrates that under reductive conditions, the increase in electrical charge (illustrated as blue curve 1) indicates that electrons are being transferred from the electrode to the melanin, and the change in optical absorbance at 570 nm (green curve 1) indicates that the melanin's redox

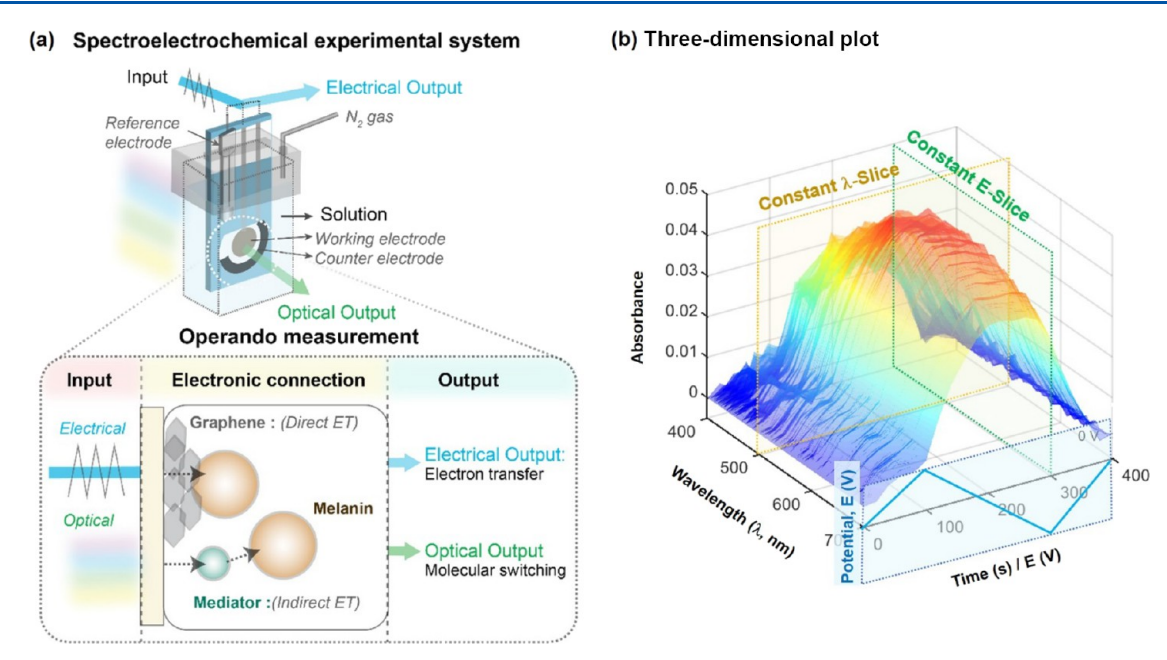


Figure 5. Description of operando measurement. (a) Schematic illustration of the operando spectroelectrochemical system to simultaneously measure the electrical and spectral responses during direct and indirect ET with melanin. (b) Three-dimensional plot showing optical absorbance as a function of the wavelength and time while a cyclic input potential was imposed to the underlying electrode.

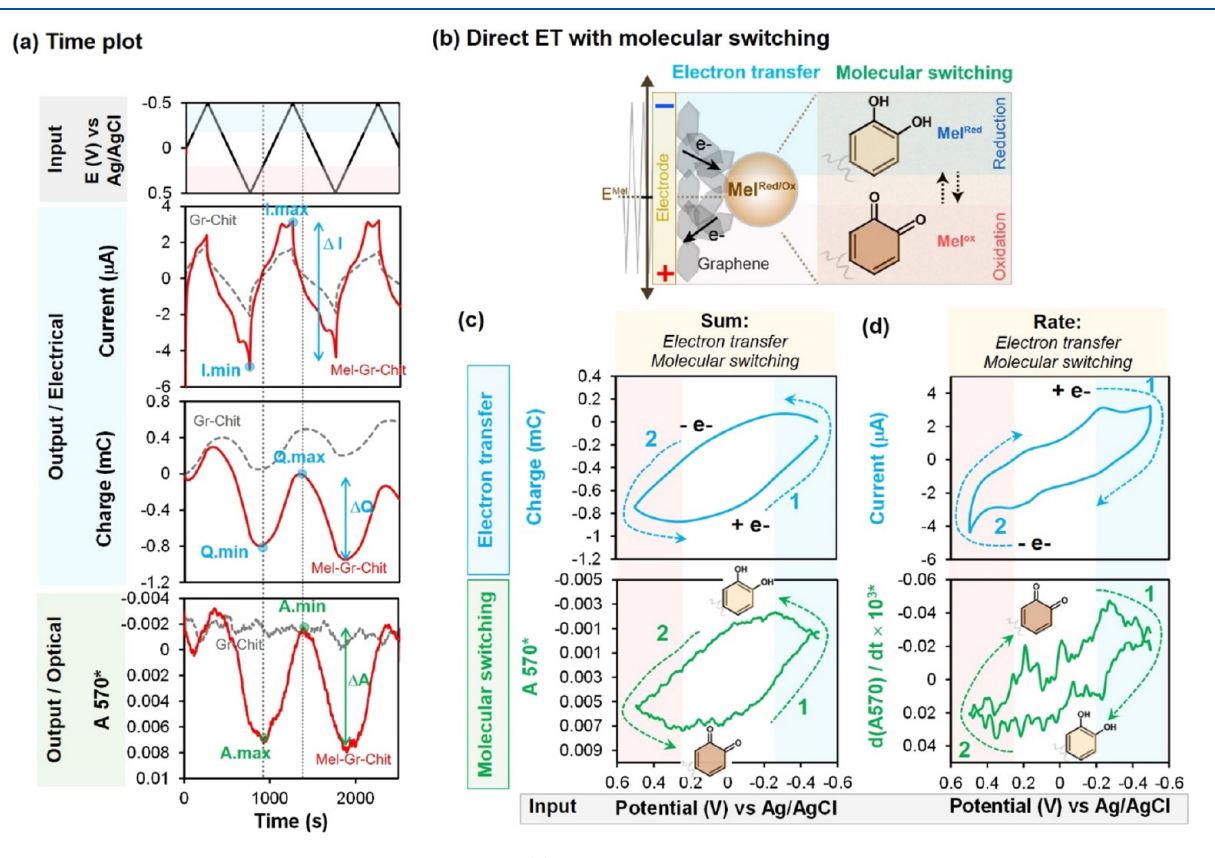


Figure 6. Direct ET and molecular switching in Mel-Gr-Chit. (a) Time-series input—output curves from operando measurements in buffered solutions without mediators using a cyclic potential (2 mV/s) imposed to the electrode coated with a 2.5 mg Mel-Gr-Chit film. (b) Schematic illustrating the electron flow and molecular switching during direct ET to melanin. (c) Phase-plane plots showing electrical charge and optical absorbance responses to the imposed input potential. (d) Phase-plane plots of the first derivatives of charge (i.e., current) and absorbance as a function of imposed input potential (the asterisk indicates that absorbance scales are inverted to facilitate comparison).

state is being switched (to presumptive catechol moieties). Under oxidative conditions highlighted in red, Figure 6c indicates that electrons flow in the opposite direction from the

melanin to the electrode (blue curve 2), and the change in optical absorbance (green curve 2) indicates that as electrons flow out of the film, the redox state of the melanin is switched

# (a) Time plot

## (b) Indirect ET with molecular switching

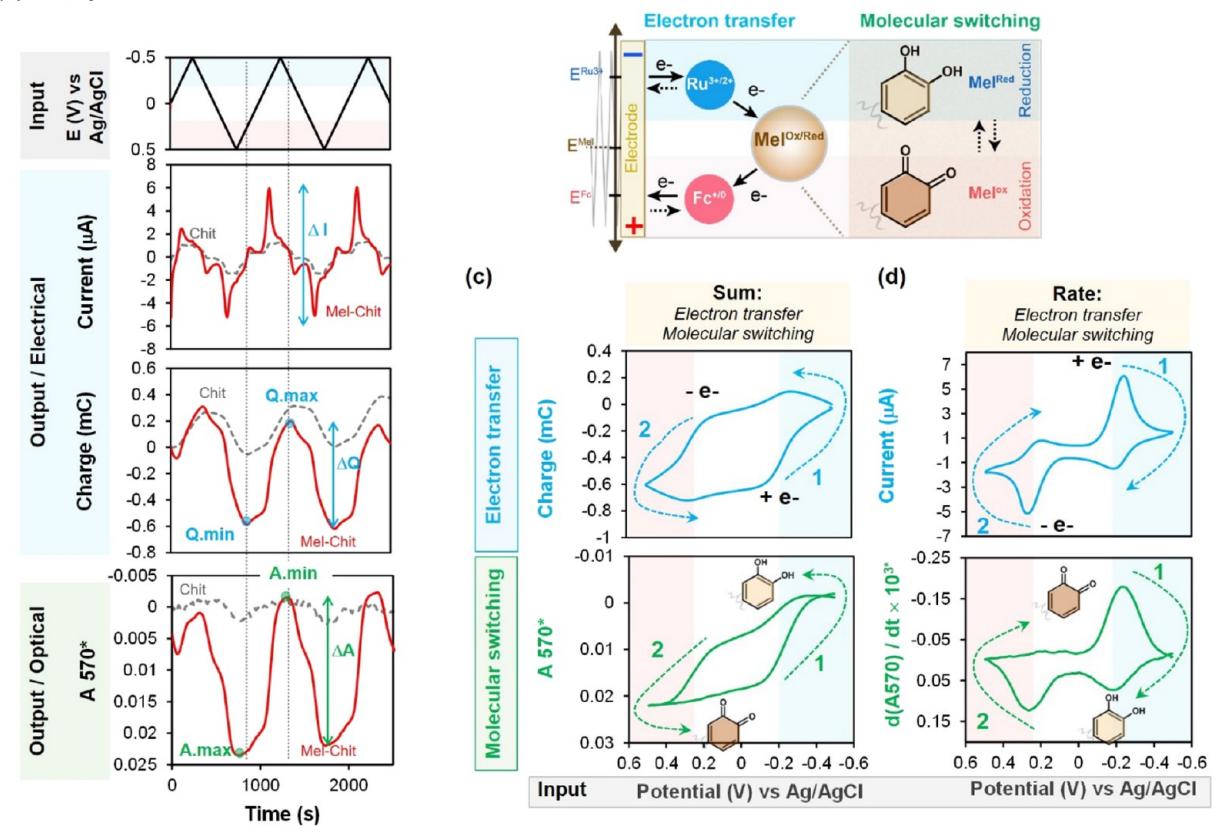


Figure 7. Indirect ET and molecular switching in Mel-Chit. (a) Time-series input—output curves from operando measurements in buffered solutions with mediators using a cyclic potential (2 mV/s) imposed to the electrode coated with a 2.5 mg Mel-Chit film. (b) Schematic illustrating the electron flow and molecular switching during indirect ET to melanin. (c) Phase-plane plots showing electrical charge and optical absorbance responses to the imposed input potential. (d) Phase-plane plots of the first derivatives of charge (i.e., current) and absorbance as a function of imposed input potential (the asterisk indicates that absorbance scales are inverted to facilitate comparison).

back (to presumptive quinone moieties). Importantly, the similarities in the shapes of the phase-plane plots in Figure 6c indicate a strong correlation between the independently measured electrical activities and molecular state changes.

Figure 6d shows additional phase-plane plots using the first derivative of the electrical and optical output signals. <sup>99,100</sup> The first derivative of the electrical charge is the current, which is the rate that electrons are being transferred to/from melanin, while the first derivative of absorbance indicates the rate of redox-state switching of the melanin. These first-derivative phase-plane plots in Figure 6d show similar features between the electrical and optical outputs, which further supports the correlation between the electron flow to/from the film and the molecular switching for BSF melanin.

In summary, the operando constant  $\lambda$  slice results of Figure 6 indicate that electrons can be directly transferred via graphene to the BSF melanin and this direct ET results in a switching of the BSF melanin's redox state.

3.3.1.2. Indirect ET with Molecular Switching. To investigate indirect ET, we prepared a Mel-Chit-coated electrode and immersed it in a cuvette containing a solution with two mediators (0.2 mM Fc and 0.2 mM Ru<sup>3+</sup>) and imposed an oscillating input potential (Figure 7a). As schematically illustrated in Figure 7b, these two mediators sequentially exchange electrons with the melanin: Ru<sup>3+</sup> undergoes reductive redox cycling that shuttles electrons from the electrode to the melanin, and Fc undergoes oxidative

redox cycling that shuttles electrons from the melanin to the electrode. Figure 7a displays the electrical and optical output responses with respect to time. As observed in Figure 7a, Mel-Chit shows an amplification in currents ( $\Delta I_{\text{Mel-Chit}} = \sim 11.06 \pm 0.04 \,\mu\text{A}$ ), which is 5-fold larger than the negative control Chit ( $\Delta I_{\text{Chit}} = \sim 2.66 \pm 0.04 \,\mu\text{A}$ ). Similarly, Figure 7a shows a 2-fold amplification of electrical charge (Q) for Mel-Chit ( $\Delta Q_{\text{Mel-Chit}} = 0.78 \pm 0.012 \,\text{mC}$ ) vs Chit ( $\Delta Q_{\text{Chit}} = 0.37 \pm 0.005 \,\text{mC}$ ) [note: Figure S4 of the Supporting Information shows the time-series outputs for the positive control film, Cat-Chit].

The last plot of Figure 7a shows a large oscillating output absorbance at 570 nm (A570) for the Mel-Chit film, while very small oscillations are apparent for the negative control film (Chit). The vertical lines of Figure 7a indicate that oscillating Q and A570 are nearly in-phase:  $Q_{\rm max}$  (reductive Q) appears at the same time as  $A_{\rm min}$  (reduced), while  $Q_{\rm min}$  (oxidative Q) occurs at approximately the same time as  $A_{\rm max}$  (oxidized). This result indicates that indirect (i.e., mediator-based) ET is correlated to the redox-state switching of the BSF melanin.

Figure 7c shows the phase-plane plots for the electrical charge (Q) and optical absorbance (A570) outputs as a function of the imposed potential (note the larger *y*-axis values in Figure 7c compared to Figure 6c). Figure 7d shows the phase-plane plots of the current and the first derivative of the absorbance. Both phase-plane plots show the consistency of electrical and optical outputs.

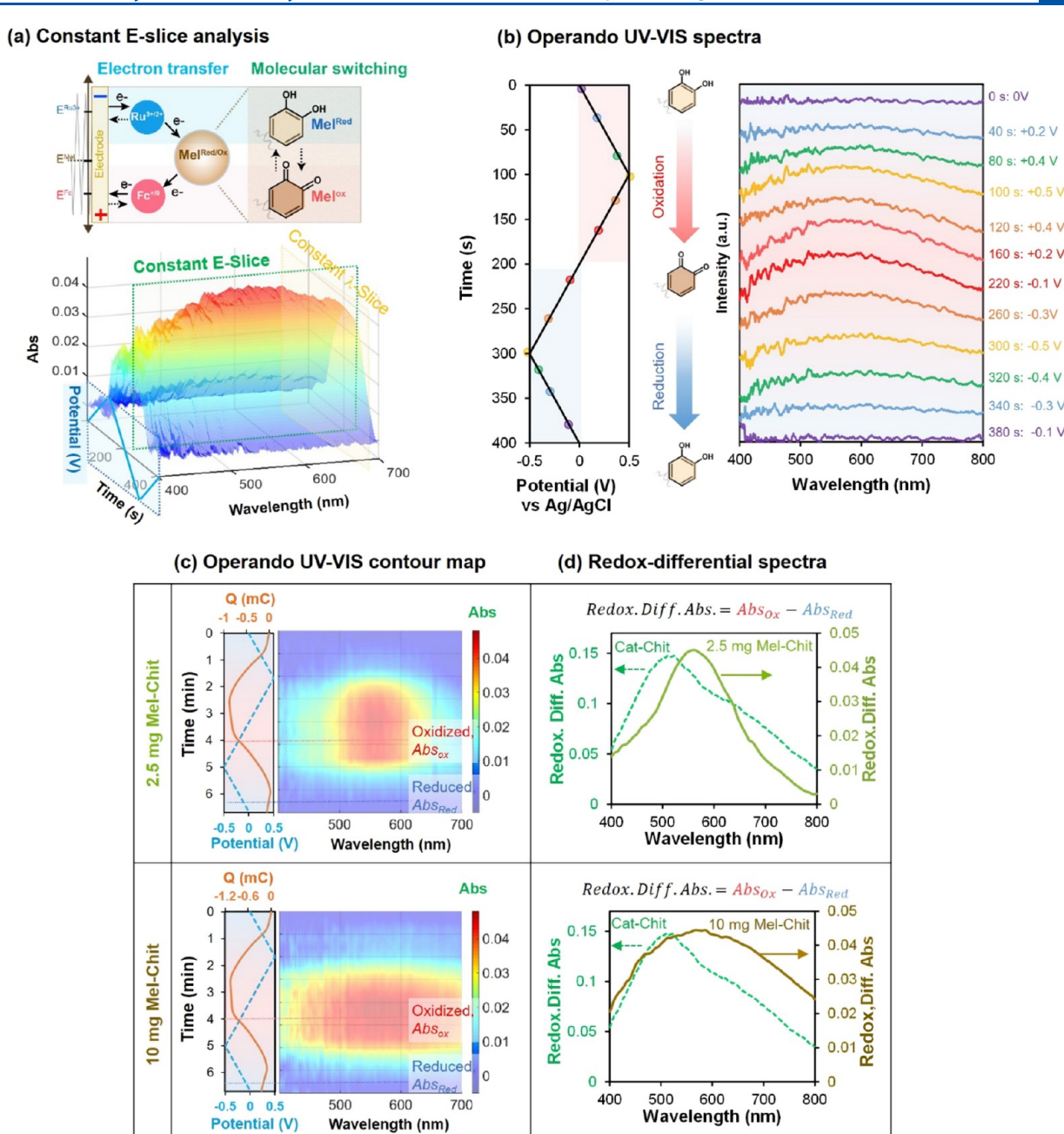


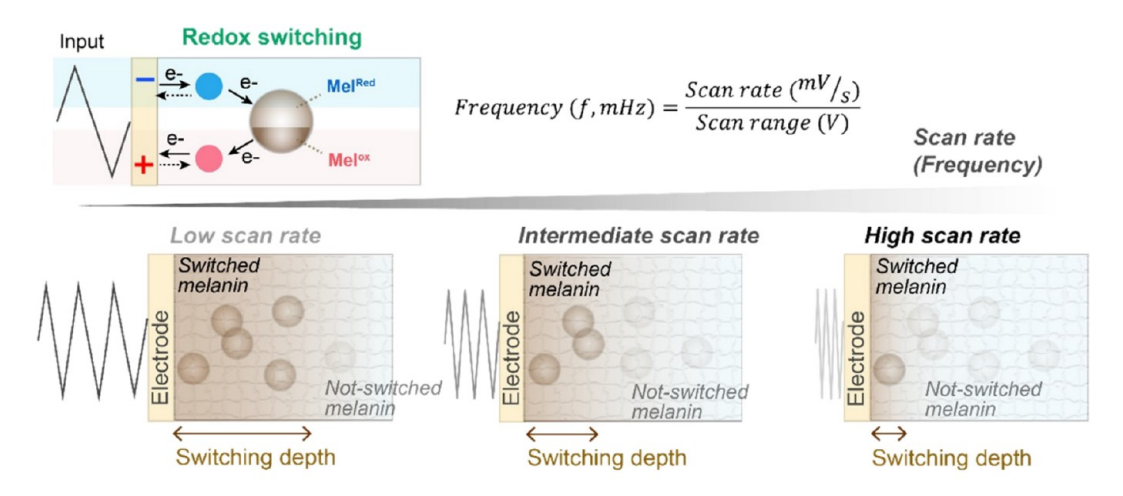
**Figure 8.** Constant *E* slice analysis showing redox-dependent spectral changes. (a) Schematic illustrating how redox-state-dependent spectral changes are revealed for a 10 mg Mel-Chit film that is being switched by an indirect ET mechanism. (b) Operando UV—vis spectra as a function of the imposed potential during one potential cycle (5 mV/s). The oxidation potential region (red shaded) shows a higher absorption than the reduction potential region (blue shaded). (c) Comparison of operando UV—vis contour maps for 2.5 and 10 mg Mel-Chit recorded during a cyclically oscillating imposed potential. The left plot shows the corresponding input potential and electrical output (charge). (d) Redox differential spectra of 2.5 and 10 mg Mel-Chit compared with Cat-Chit, showing that the change in spectral features depends on the amount of melanin and presumably its associated chemical disorder.

Additionally, we performed multicycle studies to demonstrate the repeatability of this redox-state switching for both ET pathways. Figure S5 of the Supporting Information shows that both the electrical and optical outputs repeatedly oscillated over the 9 cycles tested without a significant decay in output amplitude for Mel-Gr-Chit films in the presence or absence of mediators. These results indicate that the switching of the redox-active sites of BSF melanin (presumably switching between oxidized quinone and reduced catechol moieties) is reversible for both direct and indirect ET pathways.

In summary, the operando analysis of a constant  $\lambda$  slice indicates that an indirect (mediator-based) ET mechanism also results in a switching of the BSF melanin's redox state.

**3.3.2.** Constant *E* Slice: Redox-Dependent Spectral Changes. Figure 8a shows an operando 3D plot of a single CV potential cycle for a 10 mg Mel-Chit film measured in the presence of mediators. In this 3D plot, the constant  $\lambda$  slices focus on changes at a single wavelength to discern direct and indirect ET mechanisms, whereas constant *E* slices allow the observation of changes in the absorption spectra during redox-state switching. Figure 8b shows the operando UV—vis spectra

## (a) Frequency-dependent redox switching



### (b) Dynamic electrical and optical responses

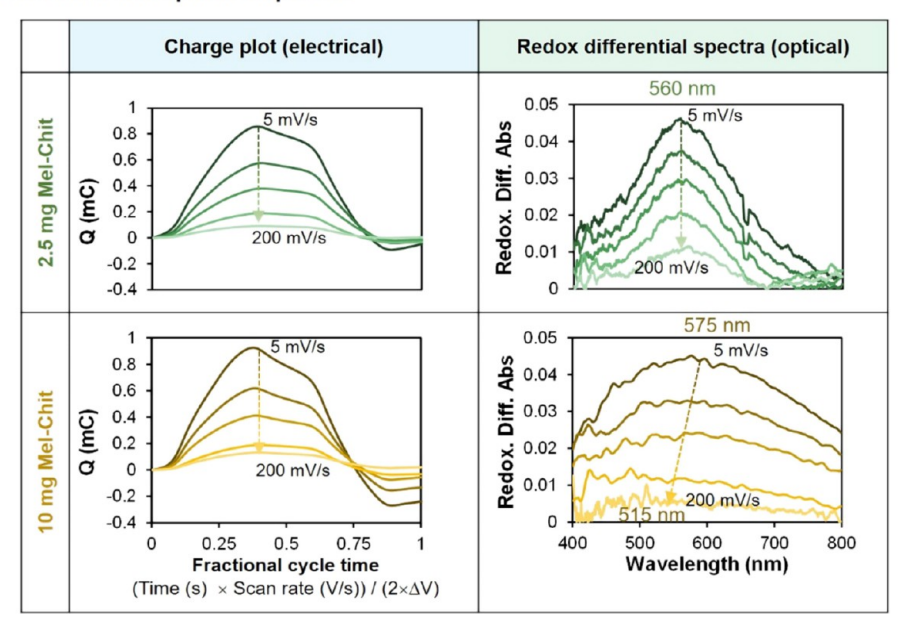


Figure 9. Dynamic operando analysis showing frequency-dependent spectroelectrochemical responses. (a) Schematic illustrating how the scan rate (or frequency) affects the distance that the mediators can penetrate into the film and exchange electrons with the grafted melanin. (b) Comparison of the dynamic electrical response (charge, Q) and optical response (redox differential spectra) for 2.5 and 10 mg Mel-Chit as a function of scan rate (from 5 to 200 mV/s). The arrows in the plots show how the peak shifts with scan rate.

of the redox switching process of Mel-Chit during a single CV cycle. As mentioned before, a spectral baseline was generated by initially poising the Mel-Chit in its reduced state by applying the reduction potential (-0.5 V) for 2 min and collecting the spectrum. During the CV measurement, the potential was scanned from 0 to 0.5 V (oxidation region; red), and the UV-vis spectra show the absorption increase between 500 and 600 nm. It indicates that Fc-oxidative redox cycling results in switching the melanin to the oxidized state. And when the scanning direction of the potential is reversed (0 to -0.5 V; reduction region; blue), the absorption gradually decreased to the baseline as melanin is converted to its reduced state by the Ru<sup>2+</sup> redox-cycling reaction. Overall, Figure 8b shows that the change in UV-vis absorbance upon melanin's redox-state switching is observed over a broad wavelength range.

Figure 8c shows the operando UV-vis contour maps of two Mel-Chit films measured during the redox-state switching. The

UV-vis contour map for the 2.5 mg Mel-Chit film shows that the absorption change occurs over a narrow range of wavelengths compared to the 10 mg Mel-Chit film [note: Figure S6 of the Supporting Information provides the UV-vis contour map of the positive control Cat-Chit film, which also shows the narrow absorption change in the lower wavelength]. As expected, both plots show that the highest absorbance (red area in the contour maps) occurs at the most oxidative Q (minimum *Q* as shown in the left plot of the contour map). To facilitate comparison, we generated a redox differential absorbance by subtracting the spectra at the reduced state ("blue dotted line") from the spectra at the oxidized state ("red dotted line"). Figure 8d shows the redox differential spectra of 2.5 and 10 mg Mel-Chit compared with Cat-Chit. One observation is that the redox differential spectra of both Mel-Chit films is red-shifted compared to that for the Cat-Chit film: this suggests that the oligomer subunits participating in the redox switching of melanin feature a more extended  $\pi$ -electron

system and may include a more diverse set of substituents compared to that of the Cat-Chit film. <sup>28,52,101</sup> A second observation is that the redox differential spectra of 10 mg Mel-Chit are broader than that of 2.5 mg Mel-Chit: possibly, the reactions associated with preparing the more concentrated Mel-Chit film increase the film's chemical disorder. <sup>56,102</sup> These results suggest that the chemical complexity of melanin is greater than that of the Cat-Chit and this complexity may depend on film preparation and increase with the amount of grafted melanin.

3.3.3. Dynamic Spectral Changes. In a final study, we performed dynamic operando analysis with Mel-Chit-coated electrodes in the presence of two mediators. The rationale for such dynamic analysis is that depending on the frequency used for probing, dynamic analysis can detect differences when phenomena occur at differing characteristic times. As illustrated in Figure 9a, probing at a low scan rate allows mediators to penetrate further from the electrode into the film to undergo indirect ET with a larger population of melanin species (compared to probing at a high scan rate). If the melanin sample being probed has significant particulate nature (e.g., Sepia melanin), then probing at high scan rates may limit mediator access to redox sites on the external surface, while probing at low scan rates may allow mediators time to penetrate deeper into the particle to access internal redoxactive moieties.<sup>88</sup> Finally, if the melanin is composed of a mixture of redox-active species, then probing at high scan rates may preferentially engage melanin's most reactive redox sites.

The plots in the first column of Figure 9b show the dynamic electrical responses for measurements with 2.5 and 10 mg Mel-Chit films. To compare plots at the same bases, we normalized the x-axis in terms of a fractional cycle time. As expected from the scheme in Figure 9a, the peaks in reductive charge (Q) decrease with increasing scan rate since the diffusion distance for the mediators decreases with scan rate. Also, as expected, the position (or imposed voltage) of the peaks in Q does not change with scan rate since these peaks reflect the reduction of the  $Ru^{3+}$  mediator.

The second column of Figure 9b compares the dynamic responses of the redox differential spectra for 2.5 and 10 mg Mel-Chit [note: Figure S7 of the Supporting Information provides the dynamic operando results for the positive control, Cat-Chit]. There are three observations from this comparison. First, as observed in Figure 8d, Figure 9b shows that the redox differential spectra for the 10 mg Mel-Chit film have a broader peak compared to that for the 2.5 mg Mel-Chit, and this broadened peak may be due to greater chemical disorder for films prepared with higher melanin contents. Second, the redox differential absorbance for both films decreases with increasing scan rate consistent with a decrease in the mediator's ability to diffuse further into the film to exchange electrons with more melanin. Finally, the variation in the shapes of the redox differential spectra with scan rate is markedly different between two Mel-Chit films. The 2.5 mg Mel-Chit film shows a peak absorption at 560 nm, and this position does not change with scan rate. In contrast, the 10 mg Mel-Chit film shows that the wavelength for peak absorption is shifted to lower wavelengths (blue-shifted) with increasing scan rates. This change in the peak position with scan rate is consistent with an explanation that different redox-active species may be undergoing ET and redox-state switching at different scan rates. While this evidence is not definitive, it is consistent with a chemical disorder model.

### 4. DISCUSSION

In this study, we investigated the electronic properties of the BSF melanin using an operando approach. This approach was possible because the BSF melanin is soluble and could be prepared in a semitransparent film that allowed simultaneous electrochemical and spectral measurements. In initial electrochemical measurements, we observed that the BSF melanin is reversibly redox active and can be repeatedly oxidized and reduced, and the BSF melanin has redox activities in the midphysiological redox potential range. These results are similar to those observed for various melanins derived from *Sepia*, fungi, and humans. <sup>87–89,103</sup>

The first conclusion from our measurements is that BSF melanin can exchange electrons through both direct and indirect ET mechanisms. Previous studies demonstrated that various natural and synthetic melanins can exchange electrons with the electrode through mediator-based indirect ET mechanisms.  $^{87-89,103}$  Here, we demonstrated that BSF melanin can be "wired" by graphene for direct ET. We believe that the direct ET between graphene and BSF melanin likely involves an extrinsic ET mechanism involving exchange between  $\pi$ -electrons of graphene and melanin.

The second conclusion is that ET through either a direct or indirect mechanism involves a change in the redox state of the BSF melanin. It is not surprising that a mediator-based indirect ET mechanism can result in a change in the redox state of melanin moieties. However, the redox-state switching observed during direct ET indicates that the electrons transferred from graphene to melanin do not necessarily continue "flowing" through the melanin but can be stored in a relatively stable redox state (depicted as a reduced catechol state). This observed redox-capacitor activity of melanin supports the hypothesis that the electrical properties of melanin are related to the redox chemistry of the constituent moieties of melanin. <sup>27,28,42</sup>

As illustrated in Scheme 1b, a chemical disorder model has been proposed to explain the broad featureless UV-vis absorbance of melanin. There are three observations from our current study that support such a chemical disorder model: (i) the "featureless" shape of the CV curve of Mel-Chit (vs Cat-Chit) in Figure 3c suggests that direct ET to BSF melanin involves multiple redox-active moieties with overlapping redox potentials; (ii) the broadening of the redox differential absorbance in Figure 8c suggests that the structure and/or interactions between moieties become more complex when films are prepared with a higher content of BSF melanin; and (iii) the frequency-dependent UV-vis spectra observed in Figure 9b suggest that the BSF melanin may have redox-active moieties that can be switched under slightly different conditions. This disorder and complexity illustrate the challenge of understanding melanin solely through bottomup chemical characterization methods. We believe that operando methods can provide a deeper understanding of the structure—activity relationship of natural melanins and various melanin-like materials <sup>104–106</sup> by detecting the structural changes that occur during electron flow.

# 5. CONCLUSIONS

We demonstrated that operando spectroelectrochemical measurements that combine UV—vis spectroscopy and electrochemistry are a powerful method to investigate the dynamic molecular changes associated with electron flow in BSF

melanin. The electrical output of the operando measurements showed that melanin could exchange electrons with electrodes via the graphene-based direct ET and mediator-based indirect ET. At the same time, the optical output showed that the electron flow of melanin through both ET pathways is accompanied by dynamic molecular changes in the oxidized and reduced states of melanin. Furthermore, these measurements support a chemical disorder model, which suggests that melanin's optical and electrical properties are affected by molecular complexities and interactions that occur over multiple length scales. Overall, we believe that operando methods provide a useful approach for characterizing melanins as they bridge traditional bottom-up chemical characterization approaches with top-down functional characterization.

# ASSOCIATED CONTENT

# **5** Supporting Information

The Supporting Information is available free of charge at https://pubs.acs.org/doi/10.1021/acs.jpcc.3c05026.

Description of the operando spectroelectrochemical system (Figure S1), additional dynamic electrochemical characterization (Figure S2), direct ET and molecular switching in Cat-Gr-Chit (Figure S3), indirect ET and molecular switching in Cat-Chit (Figure S4), stability of redox-state switching (Figure S5), comparison of operando UV—vis contour maps (Figure S6), and dynamic spectral changes of Cat-Chit (Figure S7) (PDF)

# AUTHOR INFORMATION

# **Corresponding Author**

Gregory F. Payne — Institute for Bioscience and Biotechnology Research and Robert E. Fischell Institute for Biomedical Devices, University of Maryland, College Park, Maryland 20742, United States; ⊙ orcid.org/0000-0001-6638-9459; Phone: 1-301-405-8389; Email: gpayne@umd.edu; Fax: 1-301-314-9075

# **Authors**

Eunkyoung Kim — Institute for Bioscience and Biotechnology Research and Robert E. Fischell Institute for Biomedical Devices, University of Maryland, College Park, Maryland 20742, United States; orcid.org/0000-0003-2566-4041

Chen-yu Chen – Institute for Bioscience and Biotechnology Research, Robert E. Fischell Institute for Biomedical Devices, and Fischell Department of Bioengineering, University of Maryland, College Park, Maryland 20742, United States

Jun Wei Phua – Insectta Pte. Ltd., Singapore 139954, Singapore

Alessandra Napolitano — Department of Chemical Sciences, University of Naples Federico II, I-80126 Naples, Italy; orcid.org/0000-0003-0507-5370

William E. Bentley — Institute for Bioscience and Biotechnology Research, Robert E. Fischell Institute for Biomedical Devices, and Fischell Department of Bioengineering, University of Maryland, College Park, Maryland 20742, United States; orcid.org/0000-0002-4855-7866

Complete contact information is available at: https://pubs.acs.org/10.1021/acs.jpcc.3c05026

### Notes

The authors declare no competing financial interest.

# ACKNOWLEDGMENTS

The authors acknowledge the support of the Maryland NanoCenter and its AIMLab. This work was supported by the National Science Foundation (CBET #1932963 and MCB #2227598), the Defense Threat Reduction Agency (HDTRA1-19-0021), and the Gordon and Betty Moore Foundation.

# REFERENCES

- (1) Roberts, D. D. Extracellular Matrix and Redox Signaling in Cellular Responses to Stress. *Antioxid. Redox Signaling* **2017**, 27, 771–773.
- (2) Parvez, S.; Long, M. J. C.; Poganik, J. R.; Aye, Y. Redox Signaling by Reactive Electrophiles and Oxidants. *Chem. Rev.* **2018**, *118*, 8798–8888.
- (3) Jones, R. M.; Neish, A. S. Redox Signaling Mediated by the Gut Microbiota. *Free Radical Biol. Med.* **2017**, *105*, 41–47.
- (4) Polyakov, N.; Leshina, T.; Fedenok, L.; Slepneva, I.; Kirilyuk, I.; Furso, J.; Olchawa, M.; Sarna, T.; Elas, M.; Bilkis, I.; et al. Redox-Active Quinone Chelators: Properties, Mechanisms of Action, Cell Delivery, and Cell Toxicity. *Antioxid. Redox Signaling* **2018**, 28, 1394—1403
- (5) Wang, R. S.; Oldham, W. M.; Maron, B. A.; Loscalzo, J. Systems Biology Approaches to Redox Metabolism in Stress and Disease States. *Antioxid. Redox Signaling* **2018**, *29*, 953–972.
- (6) Hansen, J. M.; Jones, D. P.; Harris, C. The Redox Theory of Development. *Antioxid. Redox Signaling* **2020**, *32*, 715–740.
- (7) Zhao, Z.; Ozcan, E. E.; VanArsdale, E.; Li, J.; Kim, E.; Sandler, A. D.; Kelly, D. L.; Bentley, W. E.; Payne, G. F. Mediated Electrochemical Probing: A Systems-Level Tool for Redox Biology. *ACS Chem. Biol.* **2021**, *16*, 1099–1110.
- (8) Pankratova, G.; Bollella, P.; Pankratov, D.; Gorton, L. Supercapacitive Biofuel Cells. *Curr. Opin. Biotechnol.* **2022**, 73, 179–187.
- (9) Mohan, A. M. V.; Rajendran, V.; Mishra, R. K.; Jayaraman, M. Recent Advances and Perspectives in Sweat Based Wearable Electrochemical Sensors. *TrAC, Trends Anal. Chem.* **2020**, *131*, 116024.
- (10) Gemünde, A.; Lai, B.; Pause, L.; Krömer, J.; Holtmann, D. Redox Mediators in Microbial Electrochemical Systems. *ChemElectroChem* **2022**, *9*, No. e202200216.
- (11) Xiao, X.; Xia, H.; Wu, R.; Bai, L.; Yan, L.; Magner, E.; Cosnier, S.; Lojou, E.; Zhu, Z.; Liu, A. Tackling the Challenges of Enzymatic (Bio)Fuel Cells. *Chem. Rev.* **2019**, *119*, 9509–9558.
- (12) Verma, J.; Kumar, D.; Singh, N.; Katti, S. S.; Shah, Y. T. Electricigens and Microbial Fuel Cells for Bioremediation and Bioenergy Production: A Review. *Environ. Chem. Lett.* **2021**, *19*, 2091–2126.
- (13) Sharova, A. S.; Melloni, F.; Lanzani, G.; Bettinger, C. J.; Caironi, M. Edible Electronics: The Vision and the Challenge. *Adv. Mater. Technol.* **2021**, *6*, 2000757.
- (14) Bandodkar, A. J.; Wang, J. Non-Invasive Wearable Electrochemical Sensors: A Review. *Trends Biotechnol.* **2014**, 363–371.
- (15) Cao, Y.; Mu, H.; Liu, W.; Zhang, R.; Guo, J.; Xian, M.; Liu, H. Electricigens in the Anode of Microbial Fuel Cells: Pure Cultures versus Mixed Communities. *Microb. Cell Fact.* **2019**, *18*, 1–14.
- (16) Logan, B. E. Exoelectrogenic Bacteria That Power Microbial Fuel Cells. *Nat. Rev. Microbiol.* **2009**, *7*, 375–381.
- (17) Rashid, R. B.; Ji, X.; Rivnay, J. Organic Electrochemical Transistors in Bioelectronic Circuits. *Biosens. Bioelectron.* **2021**, *190*, 113461.
- (18) Lovley, D. R.; Holmes, D. E. Electromicrobiology: The Ecophysiology of Phylogenetically Diverse Electroactive Microorganisms. *Nat. Rev. Microbiol.* **2022**, 20, 5–19.
- (19) Lovley, D. R. Electromicrobiology. Annu. Rev. Microbiol. 2012, 66, 391-409.

- (20) Hernandez, M. E.; Newman, D. K. Extracellular Electron Transfer. Cell. Mol. Life Sci. 2001, 58, 1562–1571.
- (21) Newman, D. K.; Kolter, R. A Role for Excreted Quinones in Extracellular Electron Transfer. *Nature* **2000**, *405*, 94–97.
- (22) Tremblay, P. L.; Angenent, L. T.; Zhang, T. Extracellular Electron Uptake: Among Autotrophs and Mediated by Surfaces. *Trends Biotechnol.* **2017**, *35*, 360–371.
- (23) Li, C.; Lesnik, K. L.; Liu, H. Stay Connected: Electrical Conductivity of Microbial Aggregates. *Biotechnol. Adv.* **2017**, *35*, 669–680.
- (24) Lovley, D. R. Happy Together: Microbial Communities That Hook up to Swap Electrons. *ISME J.* **2017**, *11*, 327–336.
- (25) Lovley, D. R. Syntrophy Goes Electric: Direct Interspecies Electron Transfer. *Annu. Rev. Microbiol.* **2017**, *71*, 643–664.
- (26) Reguera, G. Biological Electron Transport Goes the Extra Mile. *Proc. Natl. Acad. Sci. U. S. A.* **2018**, *115*, 5632–5634.
- (27) d'Ischia, M.; Napolitano, A.; Pezzella, A.; Meredith, P.; Buehler, M. Melanin Biopolymers: Tailoring Chemical Complexity for Materials Design. *Angew. Chem. Int. Ed.* **2019**, *59*, 11196–11205.
- (28) Grieco, C.; Kohl, F. R.; Hanes, A. T.; Kohler, B. Probing the Heterogeneous Structure of Eumelanin Using Ultrafast Vibrational Fingerprinting. *Nat. Commun.* **2020**, *11*, 1–9.
- (29) Reali, M.; Gouda, A.; Bellemare, J.; Ménard, D.; Nunzi, J. M.; Soavi, F.; Santato, C. Electronic Transport in the Biopigment Sepia Melanin. *ACS Appl. Bio Mater.* **2020**, *3*, 5244–5252.
- (30) Xu, R.; Gouda, A.; Caso, M. F.; Soavi, F.; Santato, C. Melanin: A Greener Route To Enhance Energy Storage under Solar Light. *ACS Omega* **2019**, *4*, 12244–12251.
- (31) Yang, L.; Guo, X.; Jin, Z.; Guo, W.; Duan, G.; Liu, X.; Li, Y. Emergence of Melanin-Inspired Supercapacitors. *Nano Today* **2021**, 37, 101075.
- (32) Kim, Y. J.; Wu, W.; Chun, S. E.; Whitacre, J. F.; Bettinger, C. J. Biologically Derived Melanin Electrodes in Aqueous Sodium-Ion Energy Storage Devices. *Proc. Natl. Acad. Sci. U. S. A.* **2013**, *110*, 20912–20917.
- (33) Camus, A.; Reali, M.; Rozel, M.; Zhuldybina, M.; Soavi, F.; Santato, C. High Conductivity Sepia Melanin Ink Films for Environmentally Benign Printed Electronics. *Proc. Natl. Acad. Sci. U. S. A.* 2022, 119, No. e2200058119.
- (34) Ail, U.; Nilsson, J.; Jansson, M.; Buyanova, I. A.; Wu, Z.; Björk, E.; Berggren, M.; Crispin, X. Optimization of Non-Pyrolyzed Lignin Electrodes for Sustainable Batteries. *Adv. Sustainable Syst.* **2023**, *7*, 2200396.
- (35) Ail, U.; Phopase, J.; Nilsson, J.; Khan, Z. U.; Inganä, O.; Berggren, M.; Crispin, X. Effect of Sulfonation Level on Lignin/Carbon Composite Electrodes for Large-Scale Organic Batteries. ACS Sustainable Chem. Eng. 2020, 8, 17933–17944.
- (36) Eliato, T. R.; Smith, J. T.; Tian, Z.; Kim, E.-S.; Hwang, W.; Andam, C. P.; Jo Kim, Y. Melanin Pigments Extracted from Horsehair as Antibacterial Agents. *J. Mater. Chem. B* **2021**, *9*, 1536–1545.
- (37) Xie, W.; Pakdel, E.; Liang, Y.; Jo Kim, Y.; Liu, D.; Sun, L.; Wang, X. Natural Eumelanin and Its Derivatives as Multifunctional Materials for Bioinspired Applications: A Review. *Biomacromolecules* **2019**, *20*, 4312–4331.
- (38) Vahidzadeh, E.; Kalra, A. P.; Shankar, K. Melanin-Based Electronics: From Proton Conductors to Photovoltaics and Beyond. *Biosens. Bioelectron.* **2018**, *122*, *127*–139.
- (39) Fahlman, M.; Fabiano, S.; Gueskine, V.; Simon, D.; Berggren, M.; Crispin, X. Interfaces in Organic Electronics. *Nat. Rev. Mater.* **2019**, *4*, 627–650.
- (40) McGinness, J.; Corry, P.; Proctor, P. Amorphous Semiconductor Switching in Melanins. *Science* **1974**, *183*, 853–855.
- (41) Bothma, J. P.; De Boor, J.; Divakar, U.; Schwenn, P. E.; Meredith, P. Device-Quality Electrically Conducting Melanin Thin Films. *Adv. Mater.* **2008**, *20*, 3539–3542.
- (42) Mostert, A. B.; Powell, B. J.; Pratt, F. L.; Hanson, G. R.; Sarna, T.; Gentle, I. R.; Meredith, P. Role of Semiconductivity and Ion Transport in the Electrical Conduction of Melanin. *Proc. Natl. Acad. Sci. U. S. A.* **2012**, *109*, 8943–8947.

- (43) Bernardus Mostert, A.; Powell, B. J.; Gentle, I. R.; Meredith, P. On the Origin of Electrical Conductivity in the Bio-Electronic Material Melanin. *Appl. Phys. Lett.* **2012**, *100*, No. 093701.
- (44) Meredith, P.; Sarna, T. The Physical and Chemical Properties of Eumelanin. *Pigm. Cell Res.* **2006**, *19*, 572–594.
- (45) Sheliakina, M.; Mostert, A. B.; Meredith, P. An All-Solid-State Biocompatible Ion-to-Electron Transducer for Bioelectronics. *Mater. Horiz.* **2018**, *5*, 256–263.
- (46) Amdursky, N.; Głowacki, E. D.; Meredith, P. Macroscale Biomolecular Electronics and Ionics. *Adv. Mater.* **2019**, *31*, 1802221.
- (47) d'Ischia, M.; Napolitano, A.; Pezzella, A.; Meredith, P.; Sarna, T. Chemical and Structural Diversity in Eumelanins: Unexplored Bio-Optoelectronic Materials. *Angew. Chem. Int. Ed.* **2009**, *48*, 3914–3921.
- (48) Meredith, P.; Bettinger, C. J.; Irimia-Vladu, M.; Mostert, A. B.; Schwenn, P. E. Electronic and Optoelectronic Materials and Devices Inspired by Nature. *Rep. Prog. Phys.* **2013**, *76*, No. 034501.
- (49) Carballo-Carbajal, I.; Laguna, A.; Romero-Giménez, J.; Cuadros, T.; Bové, J.; Martinez-Vicente, M.; Parent, A.; Gonzalez-Sepulveda, M.; Peñuelas, N.; Torra, A.; Rodríguez-Galván, B.; Ballabio, A.; Hasegawa, T.; Bortolozzi, A.; Gelpi, E.; Vila, M. Brain Tyrosinase Overexpression Implicates Age-Dependent Neuromelanin Production in Parkinson's Disease Pathogenesis. *Nat. Commun.* **2019**, *10*, 1–19.
- (50) Moreno-García, A.; Kun, A.; Calero, M.; Calero, O. The Neuromelanin Paradox and Its Dual Role in Oxidative Stress and Neurodegeneration. *Antioxidants* **2021**, *10*, 1–19.
- (51) Kim, E.; Panzella, L.; Napolitano, A.; Payne, G. F. Redox Activities of Melanins Investigated by Electrochemical Reverse Engineering: Implications for Their Roles in Oxidative Stress. *J. Invest. Dermatol.* **2020**, 140, 537–543.
- (52) Tran, M. L.; Powell, B. J.; Meredith, P. Chemical and Structural Disorder in Eumelanins: A Possible Explanation for Broadband Absorbance. *Biophys. J.* **2006**, *90*, 743–752.
- (53) Ilina, A.; Thorn, K. E.; Hume, P. A.; Wagner, I.; Tamming, R. R.; Sutton, J. J.; Gordon, K. C.; Andreassend, S. K.; Chen, K.; Hodgkiss, J. M. The Photoprotection Mechanism in the Black—Brown Pigment Eumelanin. *Proc. Natl. Acad. Sci. U. S. A.* **2022**, *119*, No. e2212343119.
- (54) D'Amora, U.; Soriente, A.; Ronca, A.; Scialla, S.; Perrella, M.; Manini, P.; Phua, J. W.; Ottenheim, C.; Di Girolamo, R.; Pezzella, A.; et al. Eumelanin from the Black Soldier Fly as Sustainable Biomaterial: Characterisation and Functional Benefits in Tissue-Engineered Composite Scaffolds. *Biomedicines* **2022**, *10*, 2945.
- (55) Prampolini, G.; Cacelli, I.; Ferretti, A. Intermolecular Interactions in Eumelanins: A Computational Bottom-up Approach. I. Small Building Blocks. *RSC Adv.* **2015**, *5*, 38513–38526.
- (56) Ju, K. Y.; Fischer, M. C.; Warren, W. S. Understanding the Role of Aggregation in the Broad Absorption Bands of Eumelanin. *ACS Nano* **2018**, *12*, 12050–12061.
- (57) Arzillo, M.; Mangiapia, G.; Pezzella, A.; Heenan, R. K.; Radulescu, A.; Paduano, L.; D'Ischia, M. Eumelanin Buildup on the Nanoscale: Aggregate Growth/Assembly and Visible Absorption Development in Biomimetic 5,6-Dihydroxyindole Polymerization. *Biomacromolecules* **2012**, *13*, 2379–2390.
- (58) Wang, Z.; Zou, Y.; Li, Y.; Cheng, Y. Metal-Containing Polydopamine Nanomaterials: Catalysis, Energy, and Theranostics. *Small* **2020**, *16*, 1907042.
- (59) Kim, Y. J.; Wu, W.; Chun, S.-E.; Whitacre, J. F.; Bettinger, C. J. Catechol-Mediated Reversible Binding of Multivalent Cations in Eumelanin Half-Cells. *Adv. Mater.* **2014**, *26*, 6572–6579.
- (60) Szpoganicz, B.; Gidanian, S.; Kong, P.; Farmer, P. Metal Binding by Melanins: Studies of Colloidal Dihydroxyindole-Melanin, and Its Complexation by Cu(II) and Zn(II) Ions. *J. Inorg. Biochem.* **2002**, *89*, 45–53.
- (61) Wahab, A.; Gogurla, N.; Park, J. Y.; Kim, S. Architecting Silk Protein and Melanin for Photoresponsive and Self-Healable Optoelectronic Skins. *Adv. Mater. Technol.* **2022**, *7*, 2101271.

- (62) Gogurla, N.; Wahab, A.; Kim, S. A Biomaterial-Silicon Junction for Photodetection. *Mater. Today Bio* **2023**, *20*, 100642.
- (63) Kumar, P.; Di Mauro, E.; Zhang, S.; Pezzella, A.; Soavi, F.; Santato, C.; Cicoira, F. Melanin-Based Flexible Supercapacitors. *J. Mater. Chem. C* **2016**, *4*, 9516–9525.
- (64) Gouda, A.; Masson, A.; Hoseinizadeh, M.; Soavi, F.; Santato, C. Biosourced Quinones for High-Performance Environmentally Benign Electrochemical Capacitors via Interface Engineering. *Commun. Chem.* **2022**, *5*, 98.
- (65) Urakawa, A. Trends and Advances in Operando Methodology. Curr. Opin. Chem. Eng. 2016, 12, 31–36.
- (66) Wu, R.; Matta, M.; Paulsen, B. D.; Rivnay, J. Operando Characterization of Organic Mixed Ionic/Electronic Conducting Materials. *Chem. Rev.* **2022**, *122*, 4493–4551.
- (67) Li, J.; Gong, J. Operando Characterization Techniques for Electrocatalysis. *Energy Environ. Sci.* **2020**, *13*, 3748.
- (68) Liu, D.; Shadike, Z.; Lin, R.; Qian, K.; Li, H.; Li, K.; Wang, S.; Yu, Q.; Liu, M.; Ganapathy, S.; et al. Review of Recent Development of In Situ/Operando Characterization Techniques for Lithium Battery Research. *Adv. Mater.* **2019**, *31*, 1806620.
- (69) de Souza, J. C. P.; Macedo, L. J. A.; Hassan, A.; Sedenho, G. C.; Modenez, I. A.; Crespilho, F. N. In Situ and Operando Techniques for Investigating Electron Transfer in Biological Systems. *ChemElectroChem* **2021**, *8*, 431–446.
- (70) Sedenho, G. C.; Hassan, A.; de Souza, J. C. P.; Crespilho, F. N. In Situ and Operando Electrochemistry of Redox Enzymes. *Curr. Opin. Electrochem.* **2022**, *34*, 101015.
- (71) Ali, M. A.; Hassan, A.; Sedenho, G. C.; Gonçalves, R. V.; Cardoso, D. R.; Crespilho, F. N. Operando Electron Paramagnetic Resonance for Elucidating the Electron Transfer Mechanism of Coenzymes. *J. Phys. Chem. C* **2019**, *123*, 16058–16064.
- (72) Phua, J. W.; Ottenheim, C. J. H. A Method for Obtaining Melanin from Inverbrate Biomass and the Product Obtained Therefrom. WO/2021/183058 A1., September 16, 2021.
- (73) Pralea, I. E.; Moldovan, R. C.; Petrache, A. M.; Ilieş, M.; Hegheş, S. C.; Ielciu, I.; Nicoară, R.; Moldovan, M.; Ene, M.; Radu, M.; et al. From Extraction to Advanced Analytical Methods: The Challenges of Melanin Analysis. *Int. J. Mol. Sci.* **2019**, *20*, 3943.
- (74) Koev, S. T.; Dykstra, P. H.; Luo, X.; Rubloff, G. W.; Bentley, W. E.; Payne, G. F.; Ghodssi, R. Chitosan: An Integrative Biomaterial for Lab-on-a-Chip Devices. *Lab Chip* **2010**, *10*, 3026–3042.
- (75) Kim, E.; Xiong, Y.; Cheng, Y.; Wu, H. C.; Liu, Y.; Morrow, B. H.; Ben-Yoav, H.; Ghodssi, R.; Rubloff, G. W.; Shen, J.; et al. Chitosan to Connect Biology to Electronics: Fabricating the Bio-Device Interface and Communicating across This Interface. *Polymers* (*Basel*). **2015**, 7, 1–46.
- (76) Wu, S.; Yan, K.; Li, J.; Huynh, R. N.; Raub, C. B.; Shen, J.; Shi, X.; Payne, G. F. Electrical Cuing of Chitosan's Mesoscale Organization. *React. Funct. Polym.* **2020**, *148*, 104492.
- (77) Kim, E.; Liu, Y.; Bentley, W. E.; Payne, G. F. Redox Capacitor to Establish Bio-Device Redox-Connectivity. *Adv. Funct. Mater.* **2012**, 22, 1409–1416.
- (78) Wu, S.; Kim, E.; Li, J.; Bentley, W. E.; Shi, X. W.; Payne, G. F. Catechol-Based Capacitor for Redox-Linked Bioelectronics. *ACS Appl. Electron. Mater.* **2019**, *1*, 1337–1347.
- (79) Kim, E.; Liu, Y.; Shi, X.-W.; Yang, X.; Bentley, W. E.; Gregory, P. F. Biomimetic Approach to Confer Redox Activity to Thin Chitosan Films. *Adv. Funct. Mater.* **2010**, *20*, 2683–2694.
- (80) Manini, P.; Lino, V.; D'Errico, G.; Reale, S.; Napolitano, A.; De Angelis, F.; d'Ischia, M. "Blackness" Is an Index of Redox Complexity in Melanin Polymers. *Polym. Chem.* **2020**, *11*, 5005–5010.
- (81) Panzella, L.; Gentile, G.; Derrico, G.; Della Vecchia, N. F.; Errico, M. E.; Napolitano, A.; Carfagna, C.; Dischia, M.; Gentile, G.; Errico, M. E.; et al. Atypical Structural and  $\pi$ -Electron Features of a Melanin Polymer That Lead to Superior Free-Radical-Scavenging Properties. *Angew. Chemie* **2013**, *125*, 12916–12919.
- (82) Wu, S.; Kim, E.; Chen, C. y.; Li, J.; VanArsdale, E.; Grieco, C.; Kohler, B.; Bentley, W. E.; Shi, X.; Payne, G. F. Catechol-Based

- Molecular Memory Film for Redox Linked Bioelectronics. Adv. Electron. Mater. 2020, 6, 2000452.
- (83) Wu, S.; Zhao, Z.; Rzasa, J. R.; Kim, E.; Li, J.; VanArsdale, E.; Bentley, W. E.; Shi, X.; Payne, G. F. Hydrogel Patterning with Catechol Enables Networked Electron Flow. *Adv. Funct. Mater.* **2021**, *31*, 2007709.
- (84) Centeno, S. A.; Shamir, J. Surface Enhanced Raman Scattering (SERS) and FTIR Characterization of the Sepia Melanin Pigment Used in Works of Art. *J. Mol. Struct.* **2008**, 873, 149–159.
- (85) Zangmeister, R. A.; Park, J. J.; Rubloff, G. W.; Tarlov, M. J. Electrochemical Study of Chitosan Films Deposited from Solution at Reducing Potentials. *Electrochim. Acta* **2006**, *51*, 5324–5333.
- (86) Zhao, Z.; Wu, S.; Kim, E.; Chen, C. Y.; Rzasa, J. R.; Shi, X.; Bentley, W. E.; Payne, G. F. System-Level Network Analysis of a Catechol Component for Redox Bioelectronics. *ACS Appl. Electron. Mater.* **2022**, *4*, 2490.
- (87) Kim, E.; Liu, Y.; Leverage, W. T.; Yin, J. J.; White, I. M.; Bentley, W. E.; Payne, G. F. Context-Dependent Redox Properties of Natural Phenolic Materials. *Biomacromolecules* **2014**, *15*, 1653–1662.
- (88) Kim, E.; Kang, M.; Tschirhart, T.; Malo, M.; Dadachova, E.; Cao, G.; Yin, J. J.; Bentley, W. E.; Wang, Z.; Payne, G. F. Spectroelectrochemical Reverse Engineering DemonstratesThat Melanin's Redox and Radical Scavenging Activities Are Linked. *Biomacromolecules* **2017**, *18*, 4084–4098.
- (89) Kim, E.; Panzella, L.; Micillo, R.; Bentley, W. E.; Napolitano, A.; Payne, G. F. Reverse Engineering Applied to Red Human Hair Pheomelanin Reveals Redox-Buffering as a Pro-Oxidant Mechanism. *Sci. Rep.* **2015**, *5*, 18447.
- (90) Kim, E.; Argenziano, R.; Zhao, Z.; Chen, C. Y.; Shen, M.; Bentley, W. E.; Napolitano, A.; Payne, G. F. Characterizing Electron Flow through Catechol-Graphene Composite Hydrogels. *Adv. Mater. Interfaces* **2022**, *9*, 2202021.
- (91) Heinze, J.; Frontana-Uribe, B. A.; Ludwigs, S. Electrochemistry of Conducting Polymers-Persistent Models and New Concepts. *Chem. Rev.* **2010**, *110*, 4724–4771.
- (92) Tsai, W. Y.; Wang, R.; Boyd, S.; Augustyn, V.; Balke, N. Probing Local Electrochemistry via Mechanical Cyclic Voltammetry Curves. *Nano Energy* **2021**, *81*, 105592.
- (93) Augustyn, V.; Come, J.; Lowe, M. A.; Kim, J. W.; Taberna, P. L.; Tolbert, S. H.; Abruña, H. D.; Simon, P.; Dunn, B. High-Rate Electrochemical Energy Storage through Li + Intercalation Pseudocapacitance. *Nat. Mater.* **2013**, *12*, 518–522.
- (94) Choi, C.; Ashby, D. S.; Butts, D. M.; DeBlock, R. H.; Wei, Q.; Lau, J.; Dunn, B. Achieving High Energy Density and High Power Density with Pseudocapacitive Materials. *Nat. Rev. Mater.* **2020**, *5*, 5–19.
- (95) Lukatskaya, M. R.; Kota, S.; Lin, Z.; Zhao, M.-Q.; Shpigel, N.; Levi, M. D.; Halim, J.; Taberna, P.-L.; Barsoum, M. W.; Simon, P.; et al. Ultra-High-Rate Pseudocapacitive Energy Storage in Two-Dimensional Transition Metal Carbides. *Nat. Energy* **2017**, *2*, 17105.
- (96) Lukatskaya, M. R.; Dunn, B.; Gogotsi, Y. Multidimensional Materials and Device Architectures for Future Hybrid Energy Storage. *Nat. Commun.* **2016**, *7*, 12647.
- (97) Mathis, T. S.; Kurra, N.; Wang, X.; Pinto, D.; Simon, P.; Gogotsi, Y. Energy Storage Data Reporting in Perspective—Guidelines for Interpreting the Performance of Electrochemical Energy Storage Systems. *Adv. Energy Mater.* **2019**, *9*, 1902007.
- (98) Ekaterina Bonaccorso, F. P.; Feng, X.; Cui, Y.; Gogotsi, Y. Energy Storage: The Future Enabled by Nanomaterials. *Science* **2019**, 366, 969.
- (99) Zhao, Z.; Kim, E.; Bentley, W. E.; Payne, G. F. Spectroelectrochemical Testing of a Proposed Mechanism for a Redox-Based Therapeutic Intervention: Ascorbate Treatment of Severe Paraquat Poisoning. Adv. Redox Res. 2023, 8, 100068.
- (100) Zhang, D.; Wang, R.; Wang, X.; Gogotsi, Y. In Situ Monitoring Redox Processes in Energy Storage Using UV–Vis Spectroscopy. *Nat. Energy* **2023**, *8*, 567–576.
- (101) Chen, C. T.; Chuang, C.; Cao, J.; Ball, V.; Ruch, D.; Buehler, M. J. Excitonic Effects from Geometric Order and Disorder Explain

- Broadband Optical Absorption in Eumelanin. *Nat. Commun.* **2014**, 5, 1-10.
- (102) Stark, K. B.; Gallas, J. M.; Zajac, G. W.; Golab, J. T.; Gidanian, S.; McIntire, T.; Farmer, P. J. Effect of Stacking and Redox State on Optical Absorption Spectra of Melanins-Comparison of Theoretical and Experimental Results. *J. Phys. Chem. B* **2005**, *109*, 1970–1977.
- (103) Kang, M.; Kim, E.; Temoçin, Z.; Li, J.; Dadachova, E.; Wang, Z.; Panzella, L.; Napolitano, A.; Bentley, W. E.; Payne, G. F. Reverse Engineering to Characterize Redox Properties: Revealing Melanin's Redox Activity through Mediated Electrochemical Probing. *Chem. Mater.* **2018**, *30*, 5814–5826.
- (104) Yang, P.; Zhu, F.; Zhang, Z.; Cheng, Y.; Wang, Z.; Li, Y. Stimuli-Responsive Polydopamine-Based Smart Materials. *Chem. Soc. Rev.* **2021**, 8319–8343.
- (105) Zhang, H.; Huang, C.; Zhang, J.; Wang, C.; Wang, T.; Shi, S.; Gu, Z.; Li, Y. Synthetic Fungal Melanin Nanoparticles with Excellent Antioxidative Property. *Giant* **2022**, *12*, 100120.
- (106) Zou, Y.; Chen, X.; Yang, P.; Liang, G.; Yang, Y.; Gu, Z.; Li, Y. Regulating the Absorption Spectrum of Polydopamine. *Sci. Adv.* **2020**, *6*, No. eabb4696.